Article

Immunity

Nanoparticle Vaccines Based on the Receptor Binding Domain (RBD) and Heptad Repeat (HR) of SARS-CoV-2 Elicit Robust Protective Immune Responses

Graphical Abstract

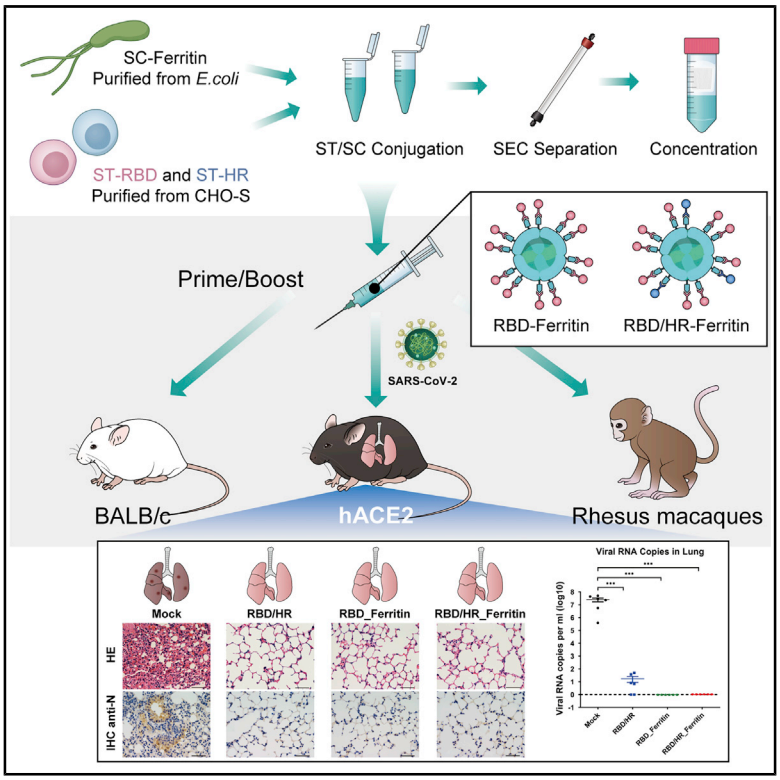

Highlights

- RBD and HR nanoparticle vaccines induce potent neutralizing antibody responses
- Nanoparticle vaccines protect against SARS-CoV-2 infection in mice
- HR antigens elicit both humoral and cellular immune responses
- HR antigens within nanoparticles contribute to cross-protective immunity

Authors

Xiancai Ma, Fan Zou, Fei Yu, ..., Ting Pan, Xin He, Hui Zhang

Correspondence

zhangh92@mail.sysu.edu.cn

In Brief

Ma et al. construct two Ferritin-based nanoparticle vaccines that conjugate RBD and HR antigens in SARS-CoV-2 Spike protein utilizing the SpyTag/SpyCatcher system. RBD and RBD-HR nanoparticles vaccines elicit more potent neutralizing antibody responses and stronger T cell immune responses than monomers. HR-containing nanoparticles induce cross-reactive immune responses against other coronaviruses.

Ma et al., 2020, Immunity *53*, 1315–1330
December 15, 2020
https://doi.org/10.1016/j.immuni.2020.11.015

CellPress

Immunity

CellPress

Article

Nanoparticle Vaccines Based on the Receptor Binding Domain (RBD) and Heptad Repeat (HR) of SARS-CoV-2 Elicit Robust Protective Immune Responses

Xiancai Ma,[1,5] Fan Zou,[2,5] Fei Yu,[3,5] Rong Li,[1,5] Yaochang Yuan,[1,5] Yiwen Zhang,[1,5] Xiantao Zhang,[1] Jieyi Deng,[1] Tao Chen,[1] Zheng Song,[1] Yidan Qiao,[1] Yikang Zhan,[1] Jun Liu,[1,2] Junsong Zhang,[3] Xu Zhang,[1] Zhilin Peng,[1] Yuzhuang Li,[1] Yingtong Lin,[1] Liting Liang,[2] Guanwen Wang,[3] Yingshi Chen,[1] Qier Chen,[1] Ting Pan,[1,4] Xin He,[1] and Hui Zhang[1,6,*]

[1]Institute of Human Virology, Key Laboratory of Tropical Disease Control of Ministry of Education, Guangdong Engineering Research Center for Antimicrobial Agent and Immunotechnology, Engineering Research Center of Gene Vaccine of Ministry of Education, Zhongshan School of Medicine, Sun Yat-sen University, Guangzhou, Guangdong, 510080, China

[2]Qianyang Biomedical Research Institute, Guangzhou, Guangdong, 510063, China

[3]Guangdong Provincial People's Hospital, Guangdong Academy of Medical Sciences, Guangzhou, Guangdong, 510080, China

[4]Center for Infection and Immunity Study, School of Medicine, Sun Yat-sen University Shenzhen, Guangdong, 518107, China

[5]These authors contributed equally

[6]Lead Contact

*Correspondence: zhangh92@mail.sysu.edu.cn

https://doi.org/10.1016/j.immuni.2020.11.015

SUMMARY

Various vaccine strategies have been proposed in response to the global COVID-19 pandemic, each with unique strategies for eliciting immune responses. Here, we developed nanoparticle vaccines by covalently conjugating the self-assembled 24-mer ferritin to the receptor binding domain (RBD) and/or heptad repeat (HR) subunits of the Severe Acute Respiratory Syndrome Coronavirus-2 (SARS-CoV-2) spike (S) protein. Compared to monomer vaccines, nanoparticle vaccines elicited more robust neutralizing antibodies and cellular immune responses. RBD and RBD-HR nanoparticle vaccinated hACE2 transgenic mice vaccinated with RBD and/or RBD-HR nanoparticles exhibited reduced viral load in the lungs after SARS-CoV-2 challenge. RBD-HR nanoparticle vaccines also promoted neutralizing antibodies and cellular immune responses against other coronaviruses. The nanoparticle vaccination of rhesus macaques induced neutralizing antibodies, and T and B cell responses prior to boost immunization; these responses persisted for more than three months. RBD- and HR-based nanoparticles thus present a promising vaccination approach against SARS-CoV-2 and other coronaviruses.

INTRODUCTION

The Coronavirus Disease 2019 (COVID-19), which is caused by Severe Acute Respiratory Syndrome Coronavirus 2 (SARS-CoV-2), has emerged as a worldwide severe pandemic and caused more than 52 million confirmed cases and more than 1 million deaths (as of middle of November 2020, report from https://covid19.who.int/) (Zhu et al., 2020b). The infection and death cases still increase rapidly for the high transmissibility with a basic reproduction number (R_0) of 3.28 and the lack of effective vaccines and therapeutic drugs (Liu et al., 2020b; Sanders et al., 2020). Developing an effective, safe, and preventative vaccine against SARS-CoV-2 is urgently needed to end the pandemic (Lurie et al., 2020).

SARS-CoV-2 is a new member of pathogenic human coronaviruses, which also includes four common coronaviruses: hCoV-NL63, hCoV-229E, hCoV-OC43, and hCoV-HKU1, and two life-threatening beta-coronaviruses SARS-CoV and MERS-CoV (Lu et al., 2020). Like other coronaviruses, SARS-CoV-2 harbors a large single-strand positive-sense genomic RNA which encodes four major structural proteins, spike (S), membrane (M), envelope (E), and nucleocapsid (N) (Shereen et al., 2020). The S protein, which contains S1 and S2 subunits, is embedded within viral envelope and mediates the recognition and entry into human cell by binding to the human angiotensin-converting enzyme 2 (hACE2) through the receptor-binding domain (RBD) within S1 subunit, followed by the fusion of viral envelope and cellular membrane through the participation of heptad repeat 1 (HR1) and heptad repeat 2 (HR2) within S2 subunit (Hoffmann et al., 2020; Walls et al., 2020). Most of the isolated neutralizing antibodies against SARS-CoV-2 infection target S protein, especially RBD (Jiang et al., 2020; Ju et al., 2020; Pinto et al., 2020; Rogers et al., 2020). Therefore, the S protein is a promising target to design candidate vaccines (Amanat and Krammer, 2020).

As of November 2020, over 259 SARS-CoV-2 vaccine candidates are under development, including 54 in clinical trials (Update on 11 November 2020, report from https://vac-lshtm.shinyapps.io/ncov_vaccine_landscape/). Most vaccine candidates target S

protein and are classified into five types: DNA vaccine, mRNA vaccine, vectored vaccine, inactivated vaccine, and protein subunit vaccine. The technique of DNA vaccine production is the simplest to obtain large amount of vaccine candidates. However, this kind of vaccination strategy is unable to totally prevent SARS-CoV-2 infection (Yu et al., 2020). mRNA vaccines, which include two candidates in phase III clinical evaluation, are also very easy to produce and have been found to prevent SARS-CoV-2 infection effectively (Erasmus et al., 2020; Jackson et al., 2020; Laczkó et al., 2020; Zhang et al., 2020a). The prophylactic effect of these mRNA vaccines will be further evaluated in clinical trials. Several reports focus on inactivated vaccines and adenovirus-vectored vaccines, including four under phase III clinical evaluation (Gao et al., 2020; Mercado et al., 2020; van Doremalen et al., 2020; Wang et al., 2020a). These reported inactivated and adenovirus-vectored vaccines prevent SARS-CoV-2 infection in animal models. However, special attention should be drawn on the potential adverse effects and moderate neutralizing antibodies (Zhu et al., 2020a). Protein subunit vaccine utilizes specific S protein or RBD protein directly without transcription or translation inside human body. Two studies utilizing disulfide-linked RBD-dimer and modified S protein-trimer, respectively, demonstrate that polymeric protein vaccines were able to induce more neutralizing antibodies than monomer vaccines (Dai et al., 2020; Tian et al., 2020; Yang et al., 2020). However, because the antigens densities of monomer, dimer and trimer are relatively less and their sizes are so small that not well compatible with the antigen capture and presentation strategy of host immune system, the immunogenicities of monomer, dimer, or trimer may still not be sufficiently robust (Shin et al., 2020; Wang et al., 2020b).

Although hundreds of SARS-CoV-2 vaccine candidates are under way, none of them has finished and passed three clinical trials to ensure its efficacy and safety as well as persistent protection. Besides, most of the ongoing vaccine investigations lack the specific enrichment of effective antigens with high immunogenicity. To overcome the above limitation and provide more alternative vaccine candidates, we designed and evaluated several nanoparticle vaccines that covalently conjugate 24 copies of RBD or RBD-HR protein subunits to the self-assembled *Helicobacter pylori* (*H. pylori*) non-haem ferritin. We investigated the total antibody and the neutralizing responses in both mice and rhesus macaques and found that ferritin-based nanoparticles were able to induce more neutralizing antibodies than protein subunit monomers. In addition, we found that the HR subunit within S2 of S protein was also able to induce notable neutralizing antibodies. The neutralizing antibody titer was further increased with HR subunit conjugation to ferritin nanoparticles. We also assessed the immunogenicity of RBD-HR chimeric ferritin nanoparticles. Both RBD nanoparticle vaccine and RBD-HR nanoparticle vaccine were able to protect virus-challenged mice against SARS-CoV-2 infection. Antibody-dependent enhancement (ADE) assay revealed that viral specific antibodies elicited by nanoparticle vaccines did not induce ADE of infection. Although the neutralizing antibody titer of RBD-HR nanoparticle was similar to RBD nanoparticle, RBD-HR nanoparticle was also able to neutralize other coronaviruses. Cellular response analysis indicated that RBD and/or HR-based nanoparticle vaccines induced stronger $CD8^+$ T cell and Th1-biased $CD4^+$ T cell responses in both mice and rhesus macaques. Collectively, the RBD and HR-based nanoparticle vaccines significantly enhance the immunogenicity.

RESULTS

RBD- and HR-based Nanoparticle Vaccine Construction and Purification

As S protein is a promising target to design vaccine candidates, we aligned the S protein sequences within mammal coronaviruses which included three SARS-CoV-2 strains (SYSU-IHV, USA-IA-6399, and Wuhan-Hu-1), the other six human pathogenic coronaviruses (SARS-CoV Tor2, MERS-CoV EMC, hCoV-HKU1, hCoV-OC43, hCoV-NL63, and hCoV-229E), five bat coronaviruses, and two pangolin coronaviruses. The alignment revealed that the heptad repeat 1 (HR1) and heptad repeat 2 (HR2) within S2 subunit was highly conserved across different SARS-CoV-2 strains and different coronaviruses genera (Figures S1A–S1D). The region of HR1-HR2 is more conservative than the receptor-binding domain (RBD) region in the evolutionary history of coronavirus (Figure S1E). RBD is also the ligand of the human angiotensin-converting enzyme 2 (hACE2) and has high immunogenicity based on the experience in SARS-CoV vaccine development (Du et al., 2009). Thus, RBD was chosen as the target of our vaccine design. Several works showed that HRs (HR1 and HR2) harbored many cross-reactive SARS-CoV-2 $CD4^+$ and $CD8^+$ T cell epitopes and had the potential to induce neutralizing responses (Ahmed et al., 2020; Elshabrawy et al., 2012; Grifoni et al., 2020a; Grifoni et al., 2020b; Mateus et al., 2020; Ravichandran et al., 2020). Especially, we recently found that 97.9% recovered COVID-19 patients exerted high titer IgG specific for HR region (Liu et al., 2020a). To extend the neutralizing spectrum, enhance T cell responses, and design a potential universal vaccine against more coronaviruses, we also chose HR as candidate to design vaccines.

To promote immunogenicity of RBD and HR-based vaccines, we intensively displayed antigens on nanoparticles. *Aquifex aeolicus* lumazine synthase (which self-assemble into 60-mer) and *Pyrococcus furiosus* ferritin (which self-assemble into 24-mer) nanoparticles have been successfully used in HIV-1 vaccine design and induced higher neutralizing responses compared with antigen monomers (Jardine et al., 2013; Tokatlian et al., 2019). Another non-haem ferritin nanoparticle, which is derived from *Helicobacter pylori* (*H. pylori*), has been successfully applied to influenza nanoparticle vaccine which elicited broadly neutralizing antibodies (Kanekiyo et al., 2013). One influenza HA *H. pylori* ferritin vaccine has completed phase I clinical trial (NCT03186781). Another *H. pylori* ferritin-based influenza H1 vaccine starts to recruit subjects (NCT03814720). Further, *H. pylori* ferritin significantly diverges from human counterparts and unlikely will induce autoantibodies. Thus, we chose *H. pylori* ferritin (hereafter ferritin) as our SARS-CoV-2 nanoparticle vaccine core. To increase the capability to present two or more different protein subunits and increase the production of subunits, we introduced the SpyTag/SpyCatcher system, which originated from *Streptococcus pyogenes,* to covalently conjugate the ferritin-based nanoparticle instead of direct fusion expression, which is much less expressed (data not shown) (Wang et al., 2020c; Zakeri et al., 2012). The SpyTag (ST) (13 aa) was genetically fused at the N terminus of RBD or HR and at the downstream of secretory signal peptide (SP) (Figure 1A). SP promoted the protein secretion and was removed after

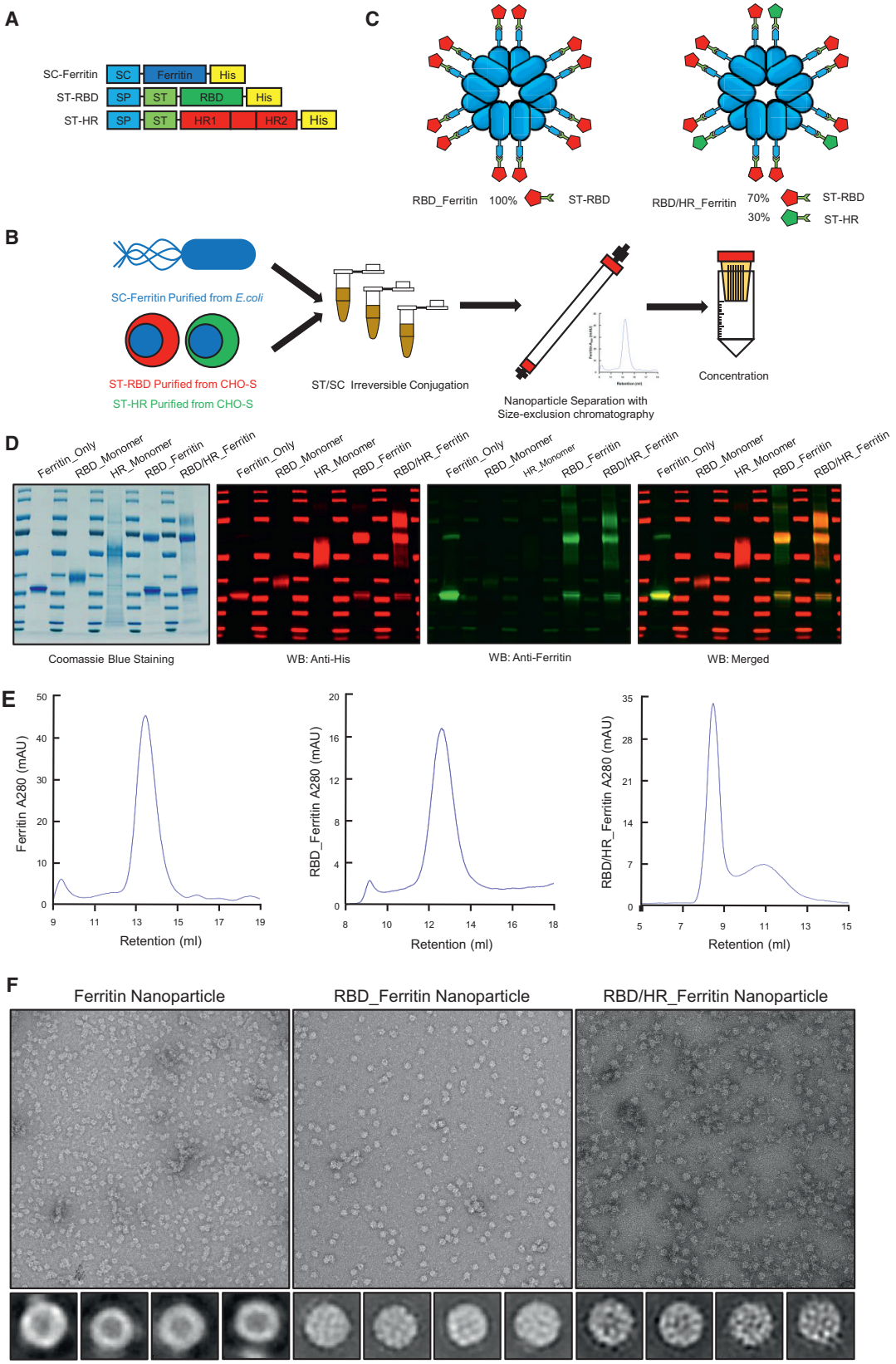

(legend on next page)

execution. SpyCatcher (SC) (138 aa) was genetically fused at the N terminus of ferritin (Figure 1A). ST-RBD, ST-HR, and SC-Ferritin were 6 × His-tagged at their C terminus to benefit affinity purification by Ni-NTA. SC-Ferritin was expressed and purified from *E.coli,* while both ST-RBD and ST-HR were expressed and purified from CHO-S cells to preserve glycosylation modifications which were vital for the immunogenicity and recognition of vaccines (Tokatlian et al., 2019; Watanabe et al., 2020). The purified SC-Ferritin core was incubated with ST-RBD and/or HR in conventional buffer without any enzyme. SC and ST formed intermolecular isopeptide bond which irreversibly conjugated Ferritin and antigen subunits. The antigen-conjugated ferritin nanoparticles were separated and collected with size-exclusion chromatography (SEC) followed by concentration (Figure 1B). To construct RBD or HR nanoparticle vaccine, each antigen was incubated with equal mole of ferritin, respectively. To construct RBD-HR chimeric nanoparticle vaccine, RBD and HR monomers were mixed in a mole ratio of 7:3, followed by incubating with ferritin (Figure 1C). The purity of ferritin core, RBD monomer, HR monomer, and corresponding nanoparticle conjugates was verified by Coomassie blue staining and western blotting (Figure 1D). The purity and homogeneity of nanoparticles was also verified by SEC and transmission electron microscopy (TEM) (Figures 1E and 1F). The mole ratio of RBD-Ferritin and HR-Ferritin within RBD-HR nanoparticles was maintained at 7:3 after SEC, based on the gradation analysis of Coomassie blue staining results. We found that SC-Ferritin core alone formed smooth spherical 24-mer nanoparticles. After antigen conjugation, RBD-Ferritin and RBD-HR-Ferritin showed spikes protruding from the spherical core (Figure 1F). Through this kind of display strategy, we successfully enriched candidate antigens in a nanoparticle.

Nanoparticle Vaccination Induces Potent Humoral Immune Responses in BALB/c Mice

To evaluate the immunogenicity of nanoparticle vaccines, six BALB/c mice were subcutaneously immunized with 10 μg dose of RBD-HR nanoparticle vaccines formulated with Sigma Adjuvant System (SAS) adjuvant (Figure 2A). Mice in the RBD nanoparticle group were immunized with equal moles of RBD-Ferritin. The moles of RBD and HR in the RBD-HR monomers group were the same as RBD-Ferritin and HR-Ferritin in the RBD-HR nanoparticle group, respectively. Mice in the RBD monomer group were immunized with equal moles of RBD as RBD-Ferritin in the RBD-HR nanoparticle group. Mice in the Ferritin group were immunized with equal moles of ferritin which were the sum of RBD-Ferritin and HR-Ferritin in the RBD-HR nanoparticle group. Equal volumes of adjuvant vaccinated mice were set as the mock group. All the mice were vaccinated with the above vaccines in a prime-boost manner, which was vaccinating mice at week 0 and week 4. Serum was collected every two weeks. Mice were euthanized at week 10. We found that the titers of RBD-specific IgG elicited by RBD and RBD-HR nanoparticle vaccines were higher than 10^5 (Figures 2B and S2A). Mice in RBD and RBD-HR monomers-vaccinated groups produced only 10^2 to 10^3 titers of RBD-specific IgG. The titers of HR-specific IgG in RBD-HR nanoparticle-vaccinated mice were similar to those in RBD-HR monomer-vaccinated mice (Figure 2C and S2B). Both titers were higher than 10^3, which indicated that HR also had a strong immunogenicity. The titers of RBD and HR antibodies were not weakened by ferritin-specific antibodies, although we also detected high titers of ferritin antibodies in ferritin-containing groups (Figures S2C and S2D). Besides, we found that the titers of RBD and HR specific antibodies in nanoparticle groups reached peak as early as two weeks post priming, which indicated that nanoparticles significantly enhanced the immunogenicity of RBD and HR antigens (Figures 2D and 2E). Because SARS-CoV-2 recognizing and entering into target cells relies on the binding of RBD to hACE2, we next tried to elucidate whether the binding of RBD to hACE2 was influenced by nanoparticles conjugation. Surface Plasmon Resonance (SPR) assay indicated that the binding of RBD-Ferritin and RBD-HR-Ferritin nanoparticles to hACE2 with affinities comparable to the binding of RBD monomer to hACE2 (Figure S2E). To further identify whether the induced antibodies were able to block RBD binding to hACE2, we conducted serum inhibition experiments. Serum from different antigen-vaccinated mice were pre-incubated with BV421-conjugated RBD protein, followed by incubating with hACE2-HeLa cells. BV421 is a polymer-based dye excited by the violet laser. The percentage of BV421-conjugated RBD-bound hACE2-HeLa cells were determined by flow cytometry. We found that antibodies from RBD-containing nanoparticle vaccine groups significantly blocked RBD binding to hACE2 (Figures S2F and S2G). The inhibitions in nanoparticles-vaccinated mice were stronger than those in RBD and RBD-HR monomers-vaccinated mice (Figure S2H).

To further evaluate the immunogenicity of nanoparticle vaccines, we conducted several neutralizing assays. We found that neutralizing antibodies (nAbs), which were induced by RBD and RBD-HR nanoparticle vaccines, strongly inhibited pseudotyped SARS-CoV-2 S/HIV-1 infection and authentic SARS-CoV-2 infection (Figures 2F and S2I). We conducted focus reduction neutralizing test (FRNT), which has been widely used to evaluate antibody and vaccine effectiveness, to verify whether nAbs induced by nanoparticle vaccines inhibit authentic SARS-CoV-2 infection

Figure 1. Construction and Purification of RBD- and HR-based Nanoparticle Vaccine

(A) Schematic of vaccine components which were 6 × His-tagged SC-Ferritin, ST-RBD and ST-HR. SC: SpyCatcher. SP: secretory signal peptide. ST: SpyTag.

(B) The procedure of nanoparticle vaccine production. SC-Ferritin was expressed and purified from *Escherichia coli (E.coli)*. ST-RBD and ST-HR were expressed and purified from CHO-S cells. SC-Ferritin and ST-RBD or ST-HR were mixed and incubated in Tris buffer to facilitate ST/SC irreversible conjugation. The conjugated nanoparticles were separated with SEC and concentrated by ultrafiltration device.

(C) Schematic illustration of Ferritin-based RBD and RBD-HR nanoparticles. RBD nanoparticle contained 100% RBD-Ferritin. RBD-HR nanoparticle contained 70% RBD-Ferritin and 30% HR-Ferritin.

(D) Coomassie blue staining and western blotting of Ferritin, RBD, HR, RBD nanoparticle, and RBD-HR nanoparticle. Both His and Ferritin antibodies were used to confirm the expression and purity of each protein.

(E) SEC of Ferritin core, RBD-Ferritin, and RBD-HR-Ferritin. The ultraviolet absorptions at 280 were shown. The retention volume represented peaks of each nanoparticles.

(F) TEM images and two-dimensional (2D) reconstruction of each nanoparticle.

See also Figure S1.

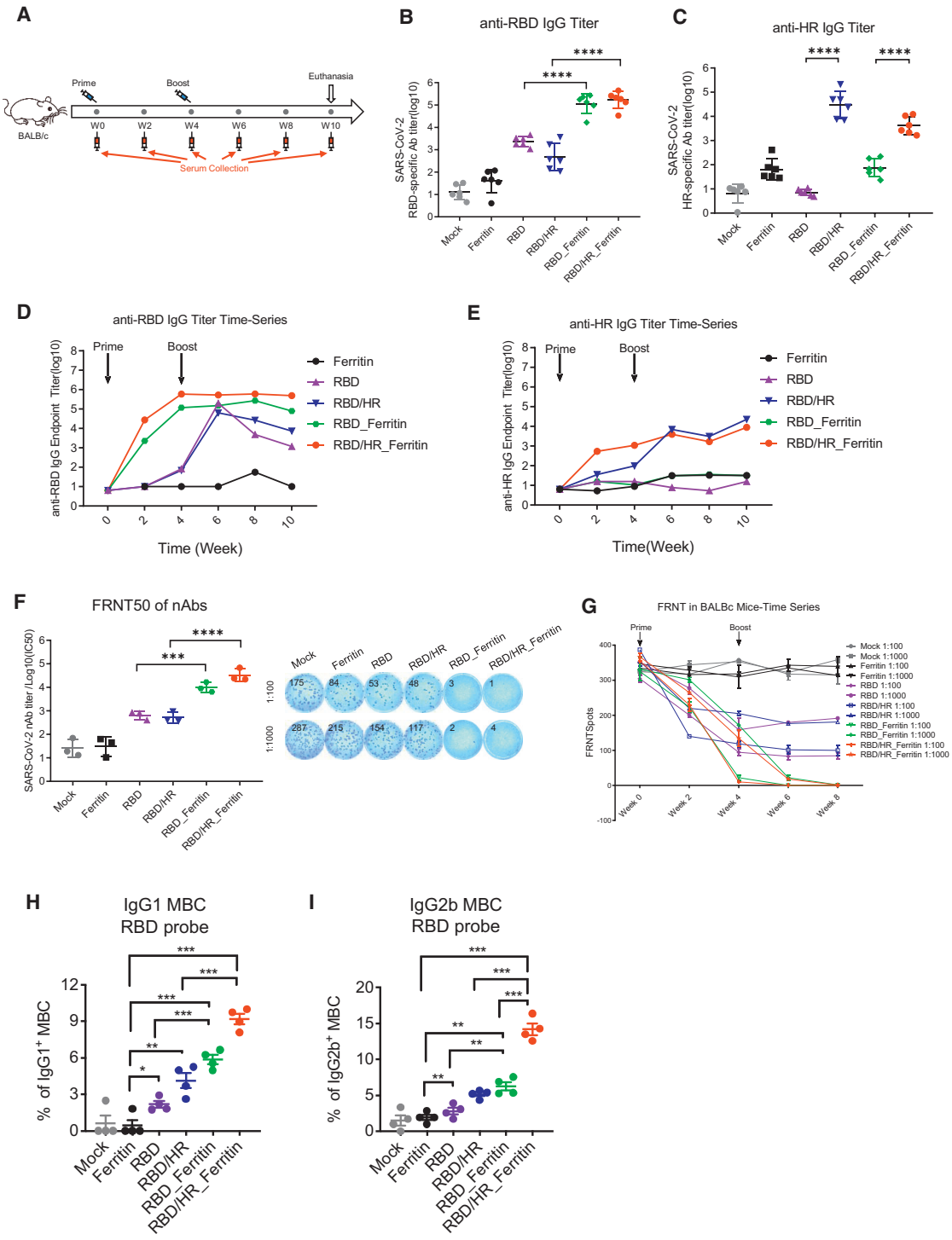

Figure 2. Humoral Immune Responses in Nanoparticles Vaccinated BALB/c Mice

(A) Schematic of BALB/c vaccination. Six mice from each group were prime/boost-vaccinated with different vaccines at week 0 and week 4. Serum was collected every two weeks. All mice were euthanized at week 10.

(B–E) SARS-CoV-2 RBD- and HR-specific IgG titers of immunized BALB/c mice at each time point were detected by ELISA. IgG antibody titers of serum which collected at week 6 were determined by serial dilution, and represented as the reciprocal of the endpoint serum dilution (B and C) (n = 6). RBD and HR-specific IgG titers in each week were calculated and plotted as time-course curve (D and E).

(F) FRNT50 of nAbs of each vaccine group was determined by FRNT and represented as half-maximal inhibitory concentrations (IC50), which was the reciprocal of half-maximal neutralizing dilution (n = 3). The right panel of (F) showed the representatives of FRNTspot wells within 1:100 and 1:1000 dilution groups.

(G) FRNTspots of serum of each time point in 1:100 and 1:1000 dilutions.

(legend continued on next page)

(Case et al., 2020; Hassan et al., 2020; Ju et al., 2020; Laczkó et al., 2020). The 50% focus reduction neutralizing test (FRNT50) titers in RBD and RBD-HR nanoparticles-vaccinated mice were over 1.4×10^4 and 3.8×10^4, respectively, which were 10- to 100- fold higher than those in RBD and RBD-HR monomers-vaccinated mice (Figure 2F). We also evaluated the neutralizing ability at different time points among different vaccine groups. The data showed that nAbs, which were elicited by nanoparticle vaccines, definitely occurred at four weeks post priming (before boost vaccination), indicating that prime-only nanoparticle vaccination strategy could be enough to elicit sufficient nAbs against SARS-CoV-2 (Figure 2G). Although monomer vaccines also elicited nAbs for authentic viruses at four weeks post prime vaccination, they did not significantly increase after boost vaccination before week 8. These results indicated that nanoparticle vaccines elicited enhanced responsed compared to monomer vaccines, both in terms of nAbs titers and the time point nAbs appeared.

To evaluate whether nanoparticle vaccines induced strong memory B cell responses, we euthanatized different vaccine-immunized BALB/c mice at six weeks post boost vaccination. Lymphocytes, which were isolated from spleen, were proceeded to evaluation for memory phenotypes. Because we have found that nanoparticle vaccines elicited higher titer of nAbs than monomer vaccines, we wondered whether the corresponding potent B cell responses could form immunological memory, the typical phenomenon of which was the generation of long-lasting memory B cells (MBCs) (Akkaya et al., 2020; Palm and Henry, 2019; Sallusto et al., 2010). We found that both RBD and RBD-HR nanoparticle vaccines generated more RBD-specific $IgG1^+$ and $IgG2b^+$ expressing MBCs compared with monomers (Figures 2H, 2I, S3A, and S3B). Based on our findings above, we concluded that nanoparticle vaccines induced higher humoral immune responses by eliciting higher titers of nAbs and more RBD-specific MBCs, which could provide persistent protective humoral responses.

Nanoparticle Vaccination Drives Type-1 T cell Responses in BALB/c Mice

The S proteins of both SARS-CoV-2 and SARS-CoV have been found to harbor multiple T cell immunogenic epitopes (Liu et al., 2017; Mateus et al., 2020). To determine whether nanoparticle vaccines also induced strong T cell responses, we analyzed different T cell population within spleen of vaccinated mice by both the enzyme-linked immune absorbent spot (ELISpot) and intracellular cytokine staining (ICCS) assays. At six weeks post boost vaccination, we found that RBD and RBD-HR nanoparticle vaccines induced higher $CD4^+$ and $CD8^+$ central memory T ($CD62L^+CD44^+$ Tcm) cells than monomer vaccines (Figures S3C and S3D). $CD4^+$ and $CD8^+$ T cell responses were evaluated by ICCS. We found that nanoparticle vaccines elicited more antigen-specific, polyfunctional $CD8^+$ T cells expressing IFN-γ^+, IL-2^+, and TNF-α^+ than the monomer vaccines (Figures 3A, 3B, 3C, and S3G). Previous studies on SARS-CoV have revealed that Type 1 T helper cell (Th1)-biased immune responses enhanced protection against virus infection, whereas Th2-biased immune responses induced vaccine-associated enhanced respiratory disease (VAERD) (Graham, 2020; Tseng et al., 2012). We measured the percentages of IFN-γ^+ $CD4^+$ T cells (Th1-biased cells) and IL-4^+ $CD4^+$ T cells (Th2-biased cells) by ICCS across different vaccine groups (Figures 3D and 3E). We found that nanoparticle vaccines induced higher Th1-biased IFN-γ^+ $CD4^+$ T cells than monomer vaccines (Figure 3D). The percentages of Th2-biased IL-4^+ $CD4^+$ T cells were no different across different groups (Figure 3E). These T cell responses were further confirmed by ELISpot assay (Figure 3F and 3G), indicating that RBD and RBD-HR nanoparticle vaccines were also able to induce strong and safe T cell immune responses apart from B cell responses.

Nanoparticle Vaccines Induce Potent Antigen Presentation and T cell–B cell Coordination

Our above results showed that nanoparticle vaccines were superior to monomer vaccines in both humoral and cellular immune responses. Previous report showed that nanoparticle vaccines are able to efficiently drain and accumulate to lymph nodes to enhance immune processing (Chattopadhyay et al., 2017). Nanoparticle vaccines were easier captured by dendritic cells (DCs) and macrophages, which facilitated T follicular helper (Tfh) cells and B cells coordination (Kelly et al., 2020; Wang et al., 2020c). To further elucidate how a nanoparticle vaccine is recognized and processed by the host immune system, we conducted several DC and macrophage antigen presentation experiments. We constructed RFP-tagged RBD monomers and RFP-tagged RBD-Ferritin nanoparticles to benefit antigen tracking. Equal moles of both antigens were subcutaneously injected to six BALB/c mice. 4 h post injection, inguinal lymph nodes were isolated, followed by obtaining DCs ($B220^-CD11c^{hi}MHC\text{-}II^+$) and macrophages ($B220^-CD11b^+F4/80^-CD169^+$) (Figures 4A and S3H). We found that the percentages of RFP-tagged RBD-Ferritin-containing DCs and macrophages were significantly higher than RFP-tagged RBD monomer-containing cells, which indicated the preferential capture of nanoparticle vaccines by DCs and macrophages (Figures 4B and 4E). The immunostaining of lymph nodes showed that RFP-tagged RBD-Ferritin antigens were significantly co-localized with macrophages in the medullary region (Figure 4F). We further verified the preferential capture of nanoparticle vaccines by DCs and the antigen presentation efficiency in healthy primary human cells *in vitro* (Zhang et al., 2020b) (Figure 4G). Mature DCs were induced from primary monocytes and then loaded with equal moles of RBD or RBD-Ferritin, followed by co-cultured with autologous $CD8^+$ T cells. S protein-specific $CD8^+$ T cells were analyzed by ELISpot. The result showed that RBD-Ferritin-incubated DCs were able to induce more IFN-γ-specific $CD8^+$ T cells than RBD-monomer-incubated cells, which indicated that the nanoparticle antigen was much easier than the monomer antigen to be captured and presented by DCs, which potently activated $CD8^+$ T cells (Figure 4H).

To verify whether nanoparticle vaccines were also easier to be captured and presented to $CD4^+$ T cells, we euthanatized vaccinated BALB/c mice ten days post vaccination and evaluated the

(H and I) The percentages of RBD-specific $IgG1^+$ and $IgG2b^+$ MBCs ($CD19^+B220^+CD38^+$) within spleen of each vaccine group (n = 4). Experiments were conducted independently in triplicates. Data represented as mean ± SEM. Adjusted p values were calculated by one-way ANOVA with Tukey's multiple comparisons test. *p < 0.05, **p < 0.01, ***p < 0.001, ****p < 0.0001.
See also Figures S2 and S3.

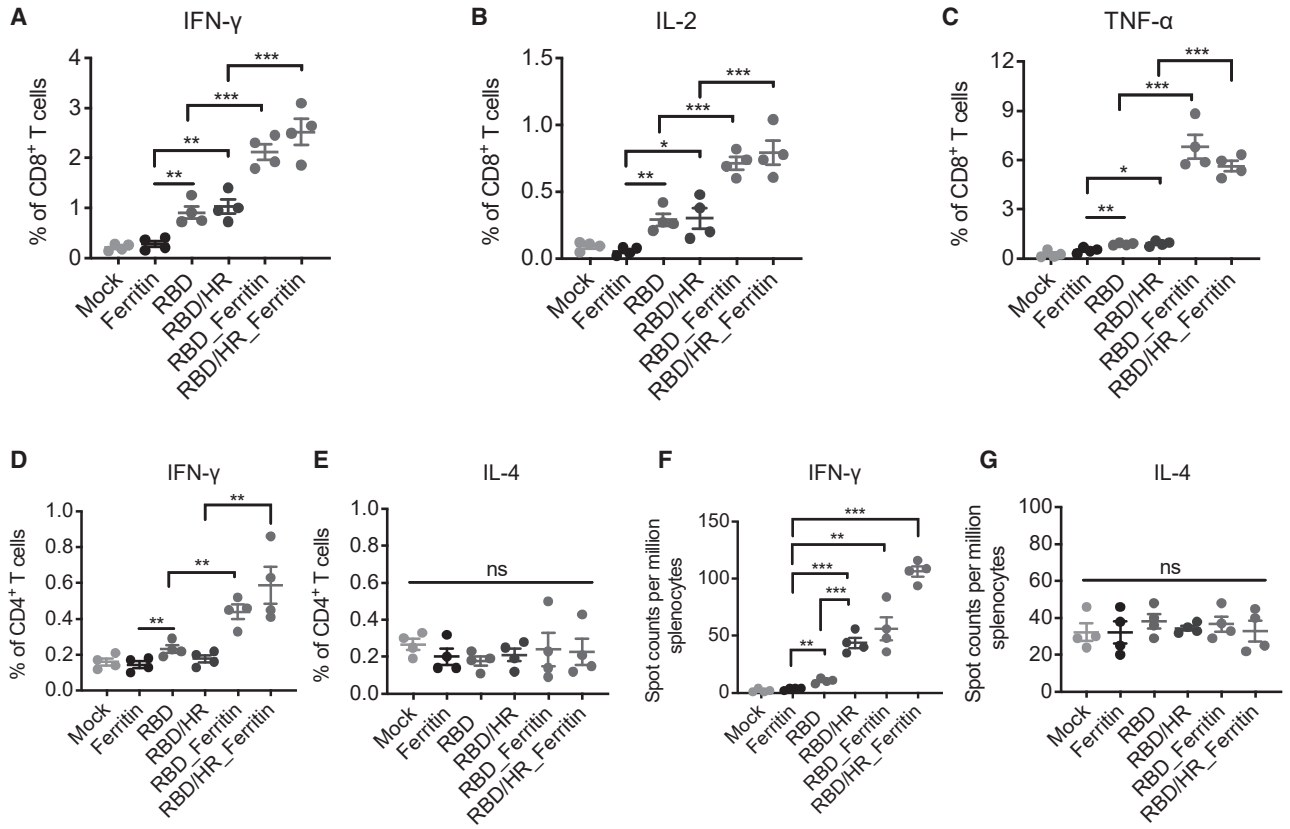

Figure 3. T Cell Immune Responses in Nanoparticles Vaccinated BALB/c Mice

(A–C) BALB/c mice were euthanized at six weeks post boost vaccination. Splenocytes were incubated with SARS-CoV-2 S peptides pool. The percentages of IFN-γ^+, IL-2^+ and TNF-α^+ $CD8^+$ T cells were determined by ICCS.

(D and E) Splenocytes were stimulated with S peptide pool as in (A). The percentages of IFN-γ^+ and IL-4^+ $CD4^+$ T cells were determined by ICCS.

(F and G) Splenocytes were stimulated with S peptide pool. ELISpot assays were conducted for IFN-γ and IL-4 secretion in splenocytes. Experiments were conducted independently in triplicates. Data represented as mean ± SEM (n = 4). Adjusted p values were calculated by one-way ANOVA with Tukey's multiple comparisons test. *$p < 0.05$, **$p < 0.01$, ***$p < 0.001$.

See also Figure S3.

percentages of different lymphocytes. We found that compared with monomers, nanoparticle vaccines elicited significant increase of activated ($CD69^+$) and antigen-experienced ($CD62L^-$ $CD44^+$) $CD4^+$ T cells (Figures S3E and S3F). Importantly, we found that the percentages of Tfh and germinal center (GC) B cells within spleen were significantly higher in nanoparticle-vaccinated mice than in monomer-vaccinated mice (Figures 4I and 4J). These results indicated that nanoparticle vaccines, especially RBD-HR chimeric nanoparticle vaccines, induced higher amounts of Tfh and GC B cells which coordinated to facilitate B cell maturation. Taken together, our results indicated that antigens associated with ferritin nanoparticle were more efficiently captured by DCs and macrophages compared with monomers, thereby enabling more effective antigen presentation and T-B cross talking in lymph nodes.

Nanoparticle Vaccines Induce Cross-Reactivity of Both Antibodies and T Cell Responses

In our alignment data, we found that HR was highly conserved across different coronaviruses (Figure S1). Both HR-containing monomers and HR-Ferritin-containing nanoparticles were able to induce high titers of HR-specific antibodies (Figures 2C, 2E and S2B). We hypothesize that HR-containing nanoparticles may also induce sufficient nAbs to neutralize other coronaviruses apart from SARS-CoV-2. We constructed an HR nanoparticle which contained 100% HR-Ferritin, and vaccinated mice with HR monomers or HR nanoparticles. Two weeks post boost, the serum of different groups was collected and used to neutralize the authentic SARS-CoV-2. The result showed that HR was able to induce nAbs, which were able to neutralize authentic viruses at 1:100 dilution (Figure 5A). HR nanoparticle vaccines induced higher nAbs than monomer (Figure 5A). We next investigated whether HR-containing vaccines induced nAbs that could neutralize other coronaviruses. We found that RBD-HR nanoparticle vaccines induced higher nAbs against pseudotyped SARS-CoV, MERS-CoV, HCoV-229E, HCoV-OC43, and RATG13, compared with monomer-induced nAbs (Figures 5B and 5F). As HR contained many T cell epitopes that could induce potent T cell responses, we next tried to investigate whether HR-containing nanoparticle vaccine-induced T cell responses were reactivated by other coronaviruses. We found that RBD-HR nanoparticle vaccine-induced T cell

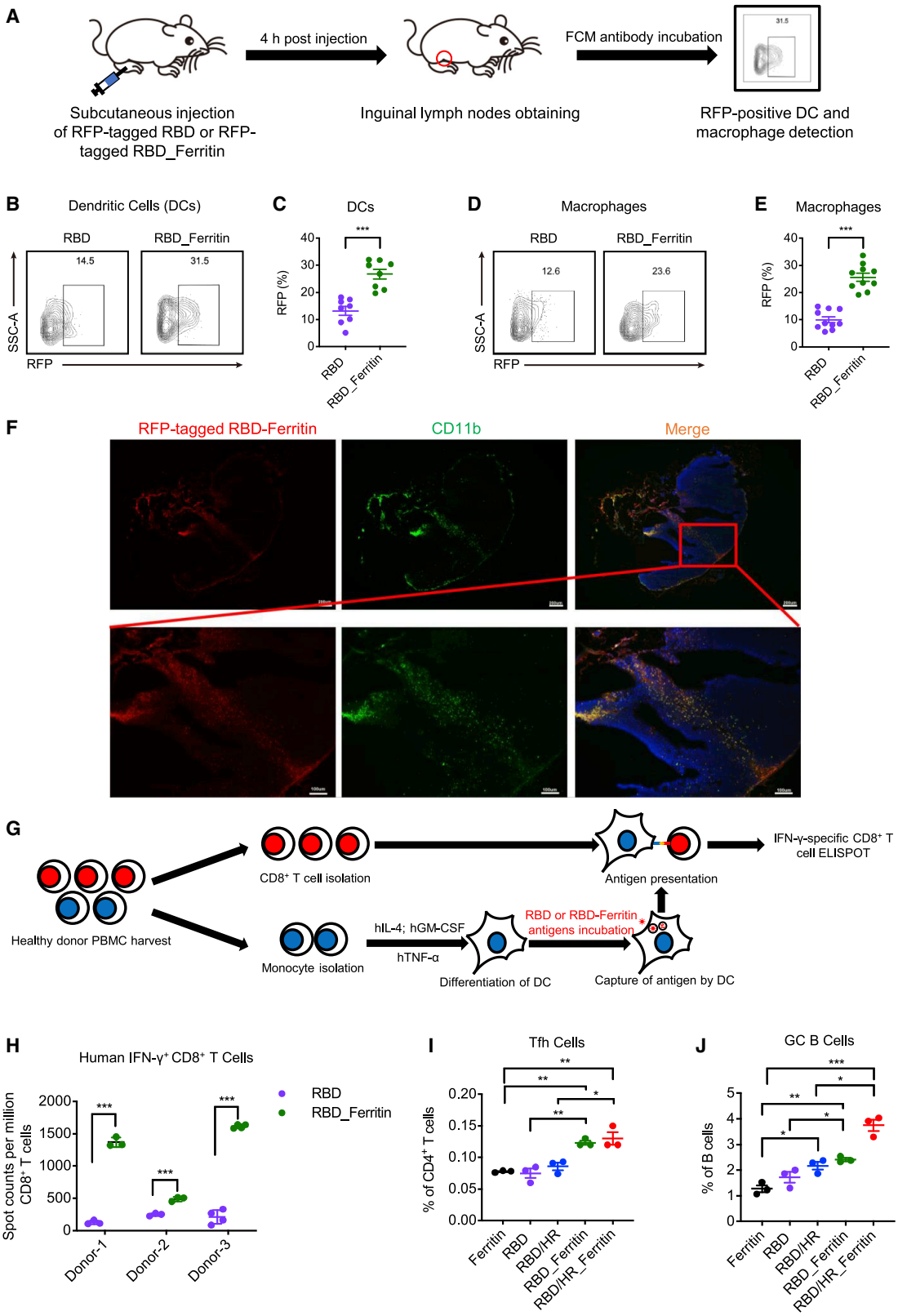

Figure 4. Potent Antigen Presentation and T-B Coordination Induced by Nanoparticle Vaccines

(A) Schematic of *in vitro* DC and macrophage antigen internalization experiment. Six C57BL/6 mice were subcutaneously injected with equal moles of RFP-tagged RBD and RFP-tagged RBD-Ferritin, both proteins were adjuvanted with SAS adjuvant. 4 h post injection, inguinal lymph nodes from both sides were

(legend continued on next page)

responses, which was represented by the IFN-γ-secreting splenocytes, were more significantly reactivated by hCoV-OC43 S peptides pool, compared with RBD nanoparticle vaccine-induced T cell responses (Figure 5G). However, the α-coronavirus hCoV-229E S peptides pool reactivated similar IFN-γ-secreting splenocytes (Figure 5H). These results indicated that HR-containing nanoparticle vaccine-elicited higher titers of nAbs and more potent T cell responses potentially cross reactivated with other β-coronaviruses.

Nanoparticle Vaccines Protect Against SARS-CoV-2 Infection in hACE2 Mice

To further investigate the immunogenicity and protection ability of nanoparticle vaccines against SARS-CoV-2, we immunized transgenic hACE2 mice which expressed humanized ACE2 receptors with RBD-HR monomers, RBD nanoparticles, and RBD-HR nanoparticles, respectively, followed by the challenge of authentic SARS-CoV-2 (Figure 6A). We found that both RBD and RBD-HR nanoparticles vaccines induced higher titers of RBD-specific IgG than RBD-HR monomer vaccine (Figures 6B and S4A). Both RBD-HR monomer vaccines and RBD-HR nanoparticle vaccines produced similar titers of HR-specific IgG (Figures 6C and S4B). Both RBD and RBD-HR nanoparticle vaccines induced high titers of ferritin-specific antibodies (Figures S4C and S4D). To evaluate whether the induced antibodies could neutralize the authentic SARS-CoV-2, we incubated the serum from vaccinated mice with authentic viruses. The serum and virus mixture was then incubated with Vero E6 cells. The efficiency of infection was determined by FRNT assay. We found that the neutralizing antibodies titers of nanoparticle vaccine groups, which were represented by FRNT50, were 100-fold higher than the monomer vaccine group (Figure 6D). The FRNT50 titers of both RBD and RBD-HR nanoparticles groups were over 2.5×10^4.

All the prime-boost-immunized mice were intranasally challenged with 4×10^4 FFU authentic SARS-CoV-2 at two weeks post boost vaccination and euthanized one week post challenge. Viral RNAs of lungs as well as the other ten tissues (myocardium, liver, spleen, kidney, cerebrum, intestine, bladder, blood, lymph node, and testis or ovary) were detected with quantitative RT-PCR. We found that the SARS-CoV-2 viral RNA copies in lungs of adjuvant-only-vaccinated mice (Mock group) were quite high (5×10^7 copies per ml) at one week post challenge (Figure 6E). A low amount of residual viral RNA was detected in the lungs of mice inoculated with RBD-HR monomer vaccine. Surprisingly, no viral RNA was detected in lungs of both RBD nanoparticle vaccine and RBD-HR nanoparticle vaccine groups, which indicated that RBD- and HR-based nanoparticle vaccines protected hACE2 mice against SARS-CoV-2 infection (Figures 6E and S4E). Histopathological analysis of lungs indicated that SARS-CoV-2 challenge induced severe lung lesions, which were characterized by thickened alveolar septa and the infiltration of inflammatory cells (Figure 6F). Nevertheless, all the lungs of monomer- and nanoparticle-vaccinated mice showed no pathological changes. Immunohistochemical assays against SARS-CoV-2 nucleocapsid (N) proteins revealed that the lungs of adjuvant-only-vaccinated mice were densely distributed with N-expressing cells, the phenomenon of which was not seen in any vaccine-immunized mice (Figure 6F). We also evaluated the pathological changes in other tissues and found that no lesion was seen in any tissues of vaccinated mice, which also indicated that vaccination by our RBD-HR monomer and corresponding nanoparticle was potentially safe (Figure S5A).

Previously, potential concerns on antibody-dependent enhancement (ADE) of infection by viral specific antibodies have been raised during flaviviruses (zika virus and dengue virus) and coronavirus (SARS-CoV-1) vaccine development (Liu et al., 2019; Shim et al., 2019; Smatti et al., 2018; Wan et al., 2020). In contrast to neutralizing antibodies, some non-neutralizing antibodies which mediated ADE promoted viral pathogenesis by infecting target cells through FcγRI/II-mediated phagocytosis. To evaluate whether antibodies elicited by nanoparticle vaccines could mediate ADE of SARS-CoV-2 infection, we mixed serially diluted serum from vaccinated mice with pseudotyped SARS-CoV-2 S/HIV-1 viruses, followed by incubating serum/virus mixtures with mouse FcγRI- and FcγRII-expressing HEK293T cells. The efficiency of infection was determined by pseudotyped virus neutralization assays. Similar system has been used to verify the safety of other SARS-CoV-2 vaccines (Laczkó et al., 2020; Quinlan et al., 2020). We found that no ADE of infection by any diluted serum was observed (Figure 6G). To verify the reliability of mFcγRI/II-HEK293T cell system, we also incubated serially diluted serum from ZIKV-infected mice with pseudotyped ZIKV S/HIV-1 virus. The serum and virus mixtures were then incubated with mFcγRI/II-HEK293T cells to determine the efficiency of infection. The results showed that anti-ZIKV serum from ZIKV-infected mice

obtained and proceeded to FCM analysis to determine the percentages of RFP-positive DCs ($B220^-CD11c^{hi}MHC\text{-}II^+$) and macrophages ($B220^-CD11b^+F4/80^-CD169^+$). (B-E) The FCM results of RFP-positive DCs and macrophages.

(B) and (D) represented the typical FCM figures.

(C) and (E) represented the statistical graphs of the FCM results (n = 8 for DCs, n = 10 for macrophages).

(F) Cryosections of inguinal lymph nodes were immunostained with antibodies against CD11b. RFP-positive cells indicated RFP-tagged RBD-Ferritin nanoparticles. The blue staining indicated DAPI-stained nuclei. Scale bars in the upper panel represented 200 μm. Scale bars in the lower panel represented 100 μm.

(G) Schematic of *in vitro* DC antigen presentation experiments. PBMCs were harvested from three healthy individuals and proceeded to monocyte isolation. Mature DCs were induced and then loaded with RBD or RBD-Ferritin antigens, followed by co-culture with autologous $CD8^+$ T cells. ELISpot assays were conducted for IFN-γ $CD8^+$ T cells.

(H) ELISpot results of *in vitro* DC antigen presentation experiment in three healthy donors (n = 3 for Donor1 and Donor 2, n = 4 for Donor 3).

(I and J) BALB/c mice were immunized with different vaccines. Ten days post immunization, mice were euthanized. The percentages of Tfh cells ($CD4^+CXCR5^+PD\text{-}1^+$) and GC B cells ($CD19^+B220^+CD95^+GL7^+$) were determined by FCM (n = 3). Experiments were conducted independently in triplicates. Data represented as mean ± SEM. P values in (C), (E), and (H) were calculated by Student's t test. Adjusted p values in (I) and (J) were calculated by one-way ANOVA with Tukey's multiple comparisons test. $^*p < 0.05$, $^{**}p < 0.01$, $^{***}p < 0.001$.

See also Figure S3.

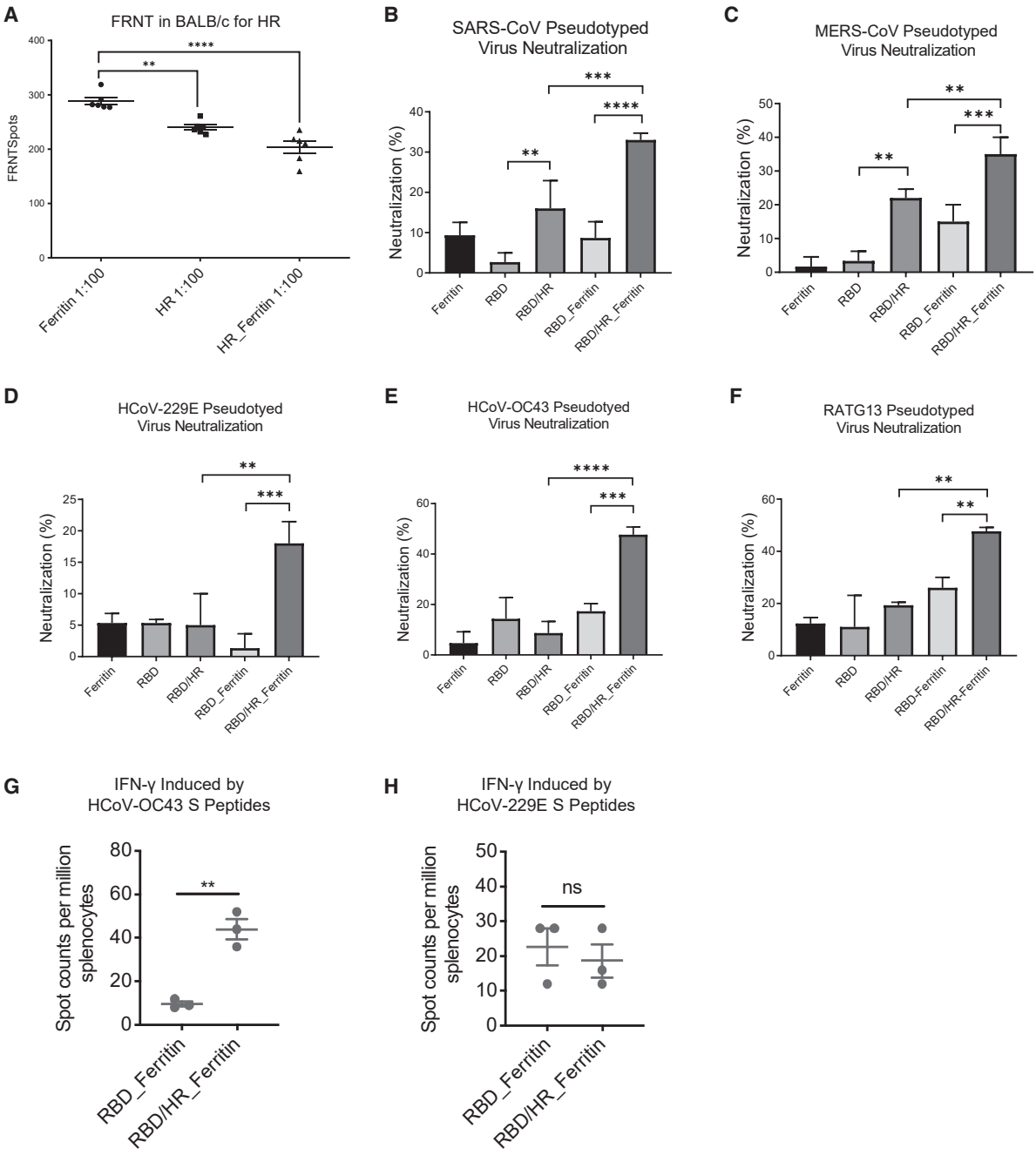

Figure 5. Cross Reactivity of Nanoparticle Vaccine-induced Antibodies and T Cell Responses

(A) Six BALB/c mice within each group were prime-boost-immunized with Ferritin core, HR monomer and HR-Ferritin nanoparticle, respectively. Serum was collected two weeks post boost vaccination and incubated with authentic SARS-CoV-2, followed by incubating with Vero E6 cells. The FRNTspots in 1:100 dilution were plotted for each group (n = 6).

(B–F) Cross-neutralization of serum of immunized BALB/c was detected with pseudotyped-CoVs which contained SARS-CoV, MERS-CoV, HCoV-229E, HCoV-OC43, and RATG13 (n = 3). Neutralizations at dilution of 1: 30 of serum were shown.

(G and H) Splenocytes of RBD and RBD-HR nanoparticle vaccines-immunized mice were incubated with hCoV-OC43 S peptides pool and hCoV-229E S peptides pool, respectively. ELISpot assay was conducted for IFN-γ secretion in splenocytes. Experiments were conducted independently in triplicates. Data represented as mean ± SEM. Adjusted p values in (A–F) were calculated by one-way ANOVA with Tukey's multiple comparisons test. P values in (G) and (H) were calculated by Student's t test. $^{**}p < 0.01$, $^{***}p < 0.001$, $^{****}p < 0.0001$.

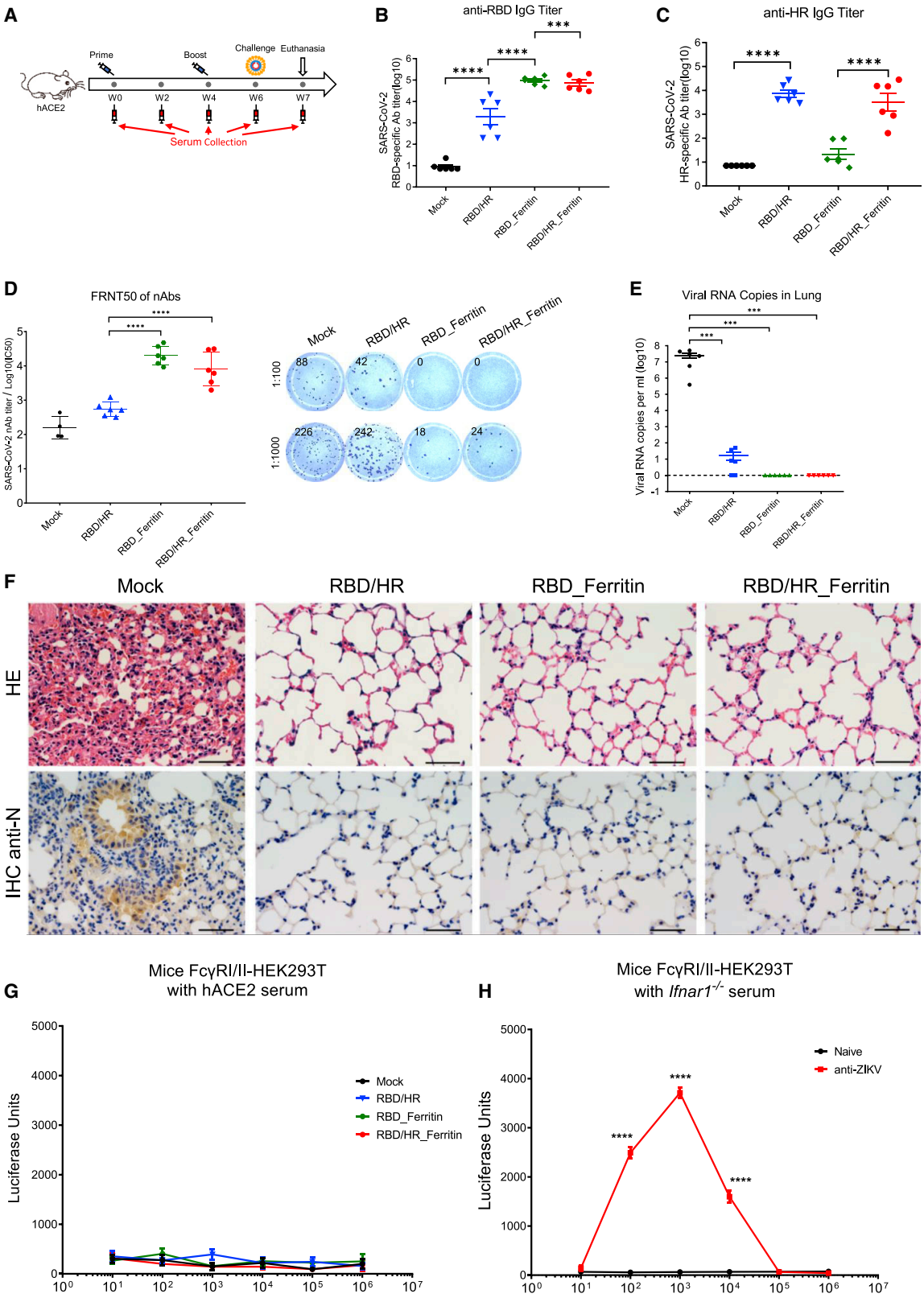

Figure 6. Protection of Nanoparticle Vaccines against SARS-CoV-2 in hACE2 Mice

(A) Schematic of hACE2 mice vaccination. Six mice within each group were prime/boost-vaccinated with different vaccines at week 0 and week 4. Two weeks post boost, mice were challenged with authentic SARS-CoV-2. All mice were euthanized one week post challenge. Serum was collected at week 0, 2, 4, 6, and 7.

(legend continued on next page)

inducted robust ADE of infection, compared with serum from naive mice (Figure 6H). Altogether, the ADE assays indicated that viral specific antibodies which elicited by nanoparticle vaccines were neutralizing without enhancing infection, which further confirmed that RBD- and HR-based nanoparticle vaccines were quite safe.

Nanoparticle Vaccines Exert Robust Immunogenicity in Rhesus Macaques

To evaluate whether nanoparticle vaccines induced prophylactic nAbs against SARS-CoV-2 in non-human primates, we immunized rhesus macaques with RBD-HR monomer, RBD nanoparticle and RBD-HR nanoparticle, respectively (Figure 7A). Nanoparticle vaccines also induced higher titers of RBD-specific IgG than monomer vaccine in rhesus macaques, the phenomenon of which have been seen in BALB/c mice and hACE2 mice (Figures 7B and S6A). The titer of HR-specific IgG in RBD-HR nanoparticle was also similar to that in RBD-HR monomers (7C and S6B). Nanoparticle vaccines also induced notable titers of ferritin-specific antibodies in rhesus macaques (Figures S6C and S6D). We assessed nAbs of each immunized rhesus macaque and found that both RBD and RBD-HR nanoparticles vaccines induced higher titer of nAbs against authentic viruses (Figure 7D and S6E) and pseudotyped SARS-CoV-2 S/HIV-1 viruses (Figure S6F) than RBD-HR monomers. The FRNT50 titers of both RBD and RBD-HR nanoparticle groups were over 4.2×10^3, which were 15-fold higher than RBD-HR monomers. Time course analysis of nAbs in each monkey showed that significant amount of nAbs against authentic viruses in nanoparticle-vaccinated monkeys appeared at two weeks post boost vaccination, and persisted for at least three months (Figure 7E). We also assessed T cell immune responses in monkey. We found that nanoparticles vaccines induced higher percentages of IFN-γ-secreting cells within PBMCs (Figure 7F), whereas the percentages of IL-4-secreting cells were similar across all the vaccination groups (Figure 7G).

To evaluate the safety of nanoparticle vaccines, we constantly conducted the physical examinations and measured blood biochemical indexes for each vaccinated rhesus macaque. We found that both prime/boost vaccinations of monomer and nanoparticle vaccines did not induce significant body temperature change (Figure S6G). The fluctuations of body weight of vaccinated monkeys in each vaccination group were also within the normal range (Figure S6H). All the serum biochemical parameters were normal across twelve weeks monitoring and showed no difference between different vaccination groups (Figure S7). We also evaluated the potential ADE of infection by serum of vaccinated rhesus macaques. Serially diluted serum was mixed with pseudotyped SARS-CoV-2 S/HIV-1 virus, followed by incubating with monkey FcγRI- and FcγRII-expressing HEK293T cells. The efficiency of infection was determined by pseudotyped virus neutralization assays. The result showed that no enhanced infection by serum of RBD-HR monomers, RBD nanoparticles and RBD-HR nanoparticles vaccinated mice was observed in any dilution (Figure 7H). These results indicated that RBD and RBD-HR nanoparticle vaccines were potentially safe and did not cause severe side effects measured by both physical examinations and blood biochemical parameters as well as ADE of infection.

DISCUSSION

In this report, we designed and evaluated two vaccines using ferritin nanoparticles conjugated with RBD or RBD-HR subunits. Both nanoparticle vaccines were able to induce abundant RBD- or HR-specific antibodies. RBD-specific antibodies of nanoparticle-vaccinated animals significantly aborted RBD-mediated hACE2 binding. Further neutralizing assays showed that nanoparticle vaccine-induced nAbs were significantly higher than monomer vaccine-induced nAbs. The nAbs induced by RBD-HR nanoparticles also neutralized other coronaviruses. The high titers of nanoparticle vaccines-induced nAbs enabled hACE2-mice totally free of SARS-CoV-2 infection upon authentic virus challenge. In addition, we found that nanoparticle vaccines induced higher percentages of cytotoxic $CD8^+$ T cells secreting IFN-γ, IL-2 and TNF-α compared to monomer vaccines, which indicated that nanoparticle vaccines were also able to activate strong T cell immune responses to eliminate the possibly infected cells. The nanoparticle vaccines induced strong protective Th1-biased responses without generating Th2-biased immune responses which may induce VAERD.

In comparison with other strategies to develop SARS-CoV-2 vaccine, nanoparticle vaccines were more easily captured and presented by DCs and macrophages. The digested antigens were then presented to $CD8^+$ T cells, which induced more IFN-γ-specific $CD8^+$ T cells. As a result, nanoparticle vaccines exert quick response of RBD- and HR-specific neutralizing antibodies and induced a higher amount of RBD-specific IgG1 and IgG2b memory B cells. The high percentage of memory

(B and C) RBD-specific and HR-specific IgG antibodies titers of serum which collected at week 6 were determined by serial dilution and represented as the reciprocal of the endpoint serum dilution (n = 6).
(D) Serum of each mice was 10-fold serially diluted and incubated with 500 FFU of authentic SARS-CoV-2, followed by incubating with Vero E6 cells. The FRNTspots of each well were counted. FRNT50 of nAbs of each vaccine group was determined by FRNT and represented as IC50 which was the reciprocal of half-maximal neutralizing dilution. The right panel showed the representatives of FRNTspot wells within 1:100 and 1:1000 dilution groups.
(E) Viral RNA copies in lung of each mice were determined by qRT-PCR and plotted as log10 copies per ml.
(F) HE staining and IHC against N proteins were evaluated in lungs of each mice.
(G) Serum of each vaccination groups was 10-fold serially diluted and mixed with pseudotyped SARS-CoV-2, followed by incubating with mFcγRI- and mFcγRII-expressing HEK293T cells. The ADE was evaluated by measuring luciferase units of each samples.
(H) Sera of naive *Ifnar1*$^{-/-}$ mice and ZIKV-infected *Ifnar1*$^{-/-}$ mice were 10-fold serially diluted and mixed with pseudotyped ZIKV. Serum/virus mixtures were incubated with mFcγRI/II-HEK293T cells. The luciferase units of each samples were measured 48 h post infection to evaluate ADE. Scale bar in (F) represented 50 μm. Experiments were conducted independently in triplicates. Data represented as mean ± SEM. Adjusted p values in (B–E) were calculated by one-way ANOVA with Tukey's multiple comparisons test. Data in (G) were analyzed by two-way ANOVA with Tukey's multiple comparisons test. Adjusted p values in (H) were calculated by two-way ANOVA with Sidak's multiple comparisons test. *$p < 0.05$, **$p < 0.01$, ***$p < 0.001$, ****$p < 0.0001$.
See also Figures S4 and S5.

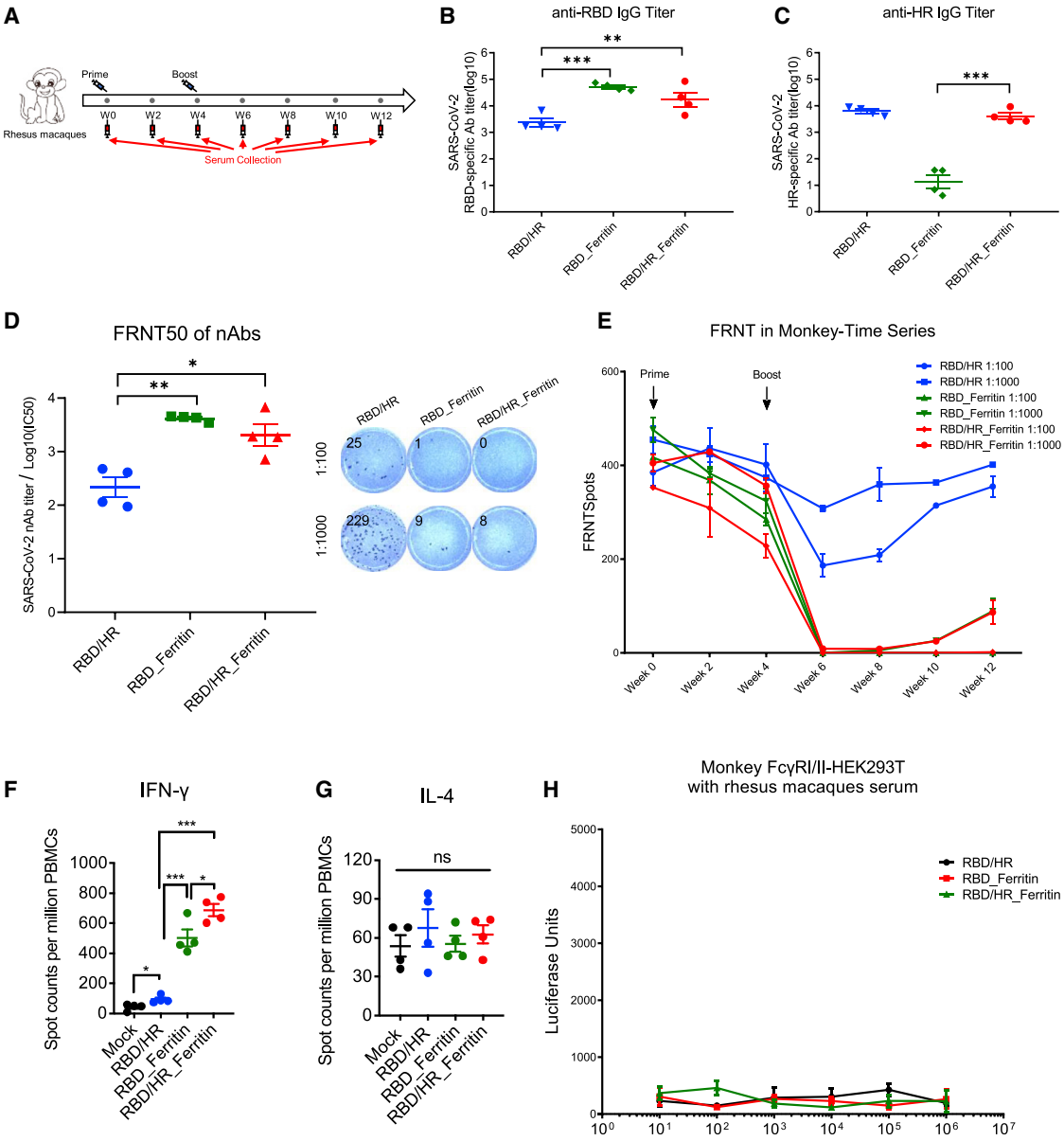

Figure 7. The Immunogenicity of Nanoparticle Vaccines in Rhesus Macaques

(A) Schematic of rhesus macaque vaccination. Twelve monkeys were prime-boost-vaccinated with RBD-HR, RBD nanoparticle and RBD-HR nanoparticle, respectively. Serum was collected every two weeks.

(B and C) RBD-specific and HR-specific IgG antibodies titers of serum which collected at week 6 were determined by serial dilution (n = 4).

(D) Serum of each monkey was 10-fold serially diluted and incubated with 500 FFU of authentic SARS-CoV-2, followed by incubating with Vero E6 cells. The FRNTspots of each well were counted. FRNT50 of nAbs of each vaccine group was determined by FRNT and represented as IC50 which was the reciprocal of half-maximal neutralizing dilution (n = 4). The right panel showed the representatives of FRNTspot wells within 1:100 and 1:1000 dilution groups (n = 4).

(E) FRNTspots of serum at each time point in 1:100 and 1:1000 dilutions.

(F and G) PBMCs of 12 vaccinated monkeys and 4 even-aged mock monkeys were collected at week 10 and incubated with S peptides pool. ELISpot assay for IFN-γ and IL-4 in PBMCs.

(H) Serum of each vaccinated monkey was 10-fold serially diluted and mixed with pseudotyped SARS-CoV-2, followed by incubating with monkey FcγRI- and monkey FcγRII-expressing HEK293T cells. The ADE of each serum was evaluated by measuring the luciferase units of each sample. Experiments were conducted independently in triplicates. Data represented as mean ± SEM. Adjusted p values in (B–D) and (F) and (G) were calculated by one-way ANOVA with Tukey's multiple comparisons test. Data in (H) were analyzed by two-way ANOVA with Tukey's multiple comparisons test. *$p < 0.05$, **$p < 0.01$, ***$p < 0.001$, ****$p < 0.0001$. See also Figures S6 and S7.

B cells in nanoparticle vaccine-immunized mice indicated that nanoparticle vaccines could induce durable humoral immune responses. In addition, small portions of S1 or S2-derived immunogens, rather than full-length S protein, exhibited by nanoparticle vaccines not only induce potent immune response, but also minimize the risk to induce ADE. Indeed, we did not find any evidence of ADE in both hACE2 mice model and rhesus macaque model. These results indicated that our vaccine strategy potentially improves the safety. Moreover, unlike other nanoparticle-derived vaccine harboring artificial materials, all the components of our nanoparticle are from nature and of high safety. Although the ferritin 24-mer core also induced ferritin-specific antibodies, the titers of RBD- or HR-specific antibodies were not significantly influenced. It is unlikely that *H. pylori* ferritin and its antibody is of obvious toxicity *in vivo*, as there have been two *H. pylori* ferritin-based influenza nanoparticle vaccines which finished or under clinical evaluations (NCT03186781, NCT03814720) and no severe side effect has been reported.

A special design for our vaccine is to add the HR subdomain in the S2 region of S protein. The homology analysis of HR region among coronaviruses indicated that HR is highly conservative in the evolutionary history of coronaviruses, especially β-coronaviruses. HR also had the potential to induce neutralizing responses (Ravichandran et al., 2020). Our nanoparticle contained HR antigens, which enabled nanoparticle vaccines to elicit substantial amount of HR-specific nAbs. Cross-neutralizing experiments showed that HR-containing nanoparticle vaccine-elicited nAbs were also able to neutralize more other coronaviruses, which indicated that utilizing HR as potent antigen to elicit nAbs could provide cross-protection against more other coronaviruses. HR region also harbors many cross-reactive SARS-CoV-2 $CD4^+$ and $CD8^+$ T cell epitopes (Ahmed et al., 2020; Grifoni et al., 2020a; Grifoni et al., 2020b; Mateus et al., 2020). We found that RBD-HR nanoparticle induced higher percentages of Tfh and B cells within germinal centers, as well as higher percentages of RBD-specific IgG1 and IgG2b memory B cells. As B cell maturation relies on the coordination with Tfh cells, it is possible that $CD4^+$ T cell epitopes within HR antigen facilitated Tfh cells to recognize and select antigen-specific B cells with high affinity, facilitating the maturation of plasma cells. Although HR-elicited nAbs were not high as those elicited by RBD, the cross-reactivity of HR-induced humoral and T cell immune responses against variable coronaviruses and the substantial contribution to T-B cell coordination motivate us to construct and evaluate coronavirus universal vaccines in the future.

Immunization with safe and efficient vaccines to achieve full protection against SARS-CoV-2 infection is urgently needed. The RBD and RBD-HR-based nanoparticle vaccines described here are of significant immunogenicity, high protection efficiency, broad spectrum, and potential safety. In addition, the generation of these nanoparticles is quite convenient. Two or three protein units can be expressed from CHO-S cells or *E.coli* in a large scale. After the expression and purification, these recombinant proteins can be mixed and automatically covalently conjugate each other to form a nanoparticle without any special enzyme and buffer. Further, no special biosafety environment concern is required for these manufacture procedures. Therefore, these nanoparticle vaccines merit being further evaluated in a Phase I-II clinical trial.

LIMITATIONS OF STUDY

Our nanoparticle vaccines study has some limitations. Although we have assessed the prophylactic effect of nanoparticle vaccines in SARS-CoV-2-challenged hACE2 mice, which could potentially mimic the prevention of vaccines for human, we have not evaluated the protection of nanoparticle vaccines against SARS-CoV-2 infection in non-human primates because of time and resource limitations. Besides, we have not tested the dose-dependent of ferritin-based nanoparticle vaccines. The dose which we used in our study was only based on the widely used monomer dose. As nanoparticle vaccines induce higher titers of nAbs than monomers, the vaccination dose of nanoparticles vaccines to induce sufficient nAbs could be lower. Nevertheless, it is still necessary to test the possible toxicity of nanoparticle vaccines at higher dose to ensure their safety. Moreover, we lack serum samples of SARS-CoV-2-infected patients to conduct FRNT50 assay, the data of which should allow a better sense of how the FRNT50 titers reported here correlate to other neutralization data reported to date.

STAR★METHODS

Detailed methods are provided in the online version of this paper and include the following:

- KEY RESOURCES TABLE
- RESOURCE AVAILABILITY
  - Lead Contact
  - Materials Availability
  - Data and Code Availability
- EXPERIMENTAL MODEL AND SUBJECT DETAILS
  - Ethics Statements
  - Cells and Viruses
  - Animal Models
- METHOD DETAILS
  - Protein Expression and Purification
  - Size-Exclusion Chromatography (SEC)
  - Transmission Electron Microscopy (TEM)
  - Animal Vaccination
  - Enzyme Linked Immunosorbent Assay (ELISA)
  - Focus Reduction Neutralizing Test (FRNT)
  - Surface Plasmon Resonance (SPR)
  - Inhibition of RBD Binding to hACE2
  - Pseudotyped Virus Neutralization Assay
  - SARS-CoV-2 Infection
  - Quantitative Reverse Transcription Polymerase Chain Reaction (qRT-PCR)
  - Splenocytes Isolation and Flow Cytometry
  - Intracellular Cytokine Staining (ICCS)
  - DC and Macrophage Studies
  - Antigen-Specific MBCs Detection
  - In vitro Antigen Presentation
  - Enzyme-Linked Immune Absorbent Spot (ELISpot) Assay
  - Histopathology and Immunohistochemistry

- Antibody-Dependent Enhancement (ADE) Assay
- Physical Examinations and Blood Biochemical Indexes in Monkeys

● QUANTIFICATION AND STATISTICAL ANALYSIS

SUPPLEMENTAL INFORMATION

Supplemental Information can be found online at https://doi.org/10.1016/j.immuni.2020.11.015.

ACKNOWLEDGMENTS

This work was supported by the National Special Research Program of China for Important Infectious Diseases (2018ZX10302103 and 2017ZX10202102), the Special 2019-nCoV Program of Natural Science Foundation of China (NSFC) (82041002), the Special 2019-nCoV Project of National Key Research and Development Program of China (2020YFC0841400), the Special 2019-nCoV Project of Research and Development Program of Guangdong (2020B111123001), the Important Key Program of NSFC (81730060), and the Joint-innovation Program in Healthcare for Special Scientific Research Projects of Guangzhou (201803040002) to H.Z. This work was also supported by the National Postdoctoral Program for Innovative Talents and the General Program of China Postdoctoral Science Foundation (BX20190398 and 2019M663215) to X.M. This work was also supported by the Pearl River S&T Nova Program of Guangzhou (201806010118) to T.P.

AUTHOR CONTRIBUTIONS

Conceptualization, X.M. and H.Z.; Methodology, X.M., F.Z., F.Y., R.L., Y.Y., Y.Z., and H.Z.; Software, X.M., R.L., X.Z., J.D., T.C., J.L., and H.Z.; Validation, X.M., F.Z., F.Y., R.L., Y.Y., Y.Z., and H.Z.; Formal Analysis, X.M., R.L., Y.Z., and H.Z.; Investigation, X.M., F.Z., F.Y., R.L., Y.Y., Y.Z., X.Z., J.D., T.C., Z.S., Y.Q., J.L., J.Z., Z.P., Y.L., L.L., G.W., Y.C., Q. C., T.P., X.H., and H.Z.; Resources, X.M., F.Z., F.Y., Y.Z., J.Z., and H.Z.; Data Curation, X.M., F.Z., X.Z., and H.Z.; Writing–Original Draft, X.M., Z.F., F.Y., R.L., Y.Y., Y.Z., and H.Z.; Writing–Review & Editing, X.M., Z.F., F.Y., R.L., Y.Y., Y.Z., and H.Z.; X.M., R.L., Y.Z., J.D., T.C, J.L., and H.Z.; Supervision, H.Z.; Project Administration, X.M., X.Z., and H.Z.; Funding Acquisition, X.M. and H.Z.

DECLARATION OF INTERESTS

X.M., F.Z., Y.Y., R.L., X.Z., and H.Z. filed patents on nanoparticle vaccines. The other authors declare no competing interests.

Received: October 11, 2020
Revised: November 16, 2020
Accepted: November 19, 2020
Published: November 25, 2020

REFERENCES

Ahmed, S.F., Quadeer, A.A., and McKay, M.R. (2020). COVIDep: a web-based platform for real-time reporting of vaccine target recommendations for SARS-CoV-2. Nat. Protoc. *15*, 2141–2142.

Akkaya, M., Kwak, K., and Pierce, S.K. (2020). B cell memory: building two walls of protection against pathogens. Nat. Rev. Immunol. *20*, 229–238.

Amanat, F., and Krammer, F. (2020). SARS-CoV-2 Vaccines: Status Report. Immunity *52*, 583–589.

Case, J.B., Rothlauf, P.W., Chen, R.E., Kafai, N.M., Fox, J.M., Shrihari, S., McCune, B.T., Harvey, I.B., Smith, B., Keeler, S.P., et al. (2020). Replication-competent vesicular stomatitis virus vaccine vector protects against SARS-CoV-2-mediated pathogenesis. Cell Host and Microbe *28*, 465–474, https://doi.org/10.1016/j.chom.2020.07.018.

Chattopadhyay, S., Chen, J.-Y., Chen, H.-W., and Hu, C.J. (2017). Nanoparticle Vaccines Adopting Virus-like Features for Enhanced Immune Potentiation. Nanotheranostics *1*, 244–260.

Dai, L., Zheng, T., Xu, K., Han, Y., Xu, L., Huang, E., An, Y., Cheng, Y., Li, S., Liu, M., et al. (2020). A Universal Design of Betacoronavirus Vaccines against COVID-19, MERS, and SARS. Cell *182*, 722–733.e11.

Du, L., He, Y., Zhou, Y., Liu, S., Zheng, B.-J., and Jiang, S. (2009). The spike protein of SARS-CoV–a target for vaccine and therapeutic development. Nat. Rev. Microbiol. *7*, 226–236.

Elshabrawy, H.A., Coughlin, M.M., Baker, S.C., and Prabhakar, B.S. (2012). Human monoclonal antibodies against highly conserved HR1 and HR2 domains of the SARS-CoV spike protein are more broadly neutralizing. PLoS ONE *7*, e50366.

Erasmus, J.H., Khandhar, A.P., O'Connor, M.A., Walls, A.C., Hemann, E.A., Murapa, P., Archer, J., Leventhal, S., Fuller, J.T., Lewis, T.B., et al. (2020). An Alphavirus-derived replicon RNA vaccine induces SARS-CoV-2 neutralizing antibody and T cell responses in mice and nonhuman primates. Science Translational Medicine *12*, https://doi.org/10.1126/SCITRANSLMED.ABC9396.

Gao, Q., Bao, L., Mao, H., Wang, L., Xu, K., Yang, M., Li, Y., Zhu, L., Wang, N., Lv, Z., et al. (2020). Development of an inactivated vaccine candidate for SARS-CoV-2. Science *369*, 77–81.

Graham, B.S. (2020). Rapid COVID-19 vaccine development. Science *368*, 945–946.

Grifoni, A., Sidney, J., Zhang, Y., Scheuermann, R.H., Peters, B., and Sette, A. (2020a). A Sequence Homology and Bioinformatic Approach Can Predict Candidate Targets for Immune Responses to SARS-CoV-2. Cell Host Microbe *27*, 671–680.e2.

Grifoni, A., Weiskopf, D., Ramirez, S.I., Mateus, J., Dan, J.M., Moderbacher, C.R., Rawlings, S.A., Sutherland, A., Premkumar, L., Jadi, R.S., et al. (2020b). Targets of T Cell Responses to SARS-CoV-2 Coronavirus in Humans with COVID-19 Disease and Unexposed Individuals. Cell *181*, 1489–1501.e15.

Hassan, A.O., Kafai, N.M., Dmitriev, I.P., Fox, J.M., Smith, B.K., Harvey, I.B., Chen, R.E., Winkler, E.S., Wessel, A.W., Case, J.B., et al. (2020). A Single-Dose Intranasal ChAd Vaccine Protects Upper and Lower Respiratory Tracts against SARS-CoV-2. Cell *183*, 169–184.e13.

Hoffmann, M., Kleine-Weber, H., Schroeder, S., Krüger, N., Herrler, T., Erichsen, S., Schiergens, T.S., Herrler, G., Wu, N.-H., Nitsche, A., et al. (2020). SARS-CoV-2 Cell Entry Depends on ACE2 and TMPRSS2 and Is Blocked by a Clinically Proven Protease Inhibitor. Cell *181*, 271–280.e8.

Jackson, L.A., Anderson, E.J., Rouphael, N.G., Roberts, P.C., Makhene, M., Coler, R.N., McCullough, M.P., Chappell, J.D., Denison, M.R., Stevens, L.J., et al. (2020). An mRNA Vaccine against SARS-CoV-2 — Preliminary Report. New England Journal of Medicine.

Jardine, J., Julien, J.-P., Menis, S., Ota, T., Kalyuzhniy, O., McGuire, A., Sok, D., Huang, P.-S., MacPherson, S., Jones, M., et al. (2013). Rational HIV immunogen design to target specific germline B cell receptors. Science *340*, 711–716.

Jiang, S., Hillyer, C., and Du, L. (2020). Neutralizing Antibodies against SARS-CoV-2 and Other Human Coronaviruses. Trends Immunol. *41*, 355–359.

Ju, B., Zhang, Q., Ge, J., Wang, R., Sun, J., Ge, X., Yu, J., Shan, S., Zhou, B., Song, S., et al. (2020). Human neutralizing antibodies elicited by SARS-CoV-2 infection. Nature *584*, 115–119.

Kanekiyo, M., Wei, C.-J., Yassine, H.M., McTamney, P.M., Boyington, J.C., Whittle, J.R.R., Rao, S.S., Kong, W.-P., Wang, L., and Nabel, G.J. (2013). Self-assembling influenza nanoparticle vaccines elicit broadly neutralizing H1N1 antibodies. Nature *499*, 102–106.

Kelly, H.G., Tan, H.-X., Juno, J.A., Esterbauer, R., Ju, Y., Jiang, W., Wimmer, V.C., Duckworth, B.C., Groom, J.R., Caruso, F., et al. (2020). Self-assembling influenza nanoparticle vaccines drive extended germinal center activity and memory B cell maturation. JCI Insight *5*, e136653.

Laczkó, D., Hogan, M.J., Toulmin, S.A., Hicks, P., Lederer, K., Gaudette, B.T., Castaño, D., Amanat, F., Muramatsu, H., Oguin, T.H., 3rd, et al. (2020). A single immunization with nucleoside-modified mRNA vaccines elicits strong cellular and humoral immune responses against SARS-CoV-2 in mice. Immunity *53*, 724–732.e7.

Liu, W.J., Zhao, M., Liu, K., Xu, K., Wong, G., Tan, W., and Gao, G.F. (2017). T-cell immunity of SARS-CoV: Implications for vaccine development against MERS-CoV. Antiviral Res. *137*, 82–92.

Liu, L., Wei, Q., Lin, Q., Fang, J., Wang, H., Kwok, H., Tang, H., Nishiura, K., Peng, J., Tan, Z., et al. (2019). Anti-spike IgG causes severe acute lung injury by skewing macrophage responses during acute SARS-CoV infection. JCI Insight *4*, e123158.

Liu, B., Shi, Y., Zhang, W., Li, R., He, Z., Yang, X., Pan, Y., Deng, X., Tan, M., Zhao, L., et al. (2020a). Recovered COVID-19 patients with recurrent viral RNA exhibit lower levels of anti-RBD antibodies. Cell. Mol. Immunol. *17*, 1098–1100.

Liu, Y., Gayle, A.A., Wilder-Smith, A., and Rocklöv, J. (2020b). The reproductive number of COVID-19 is higher compared to SARS coronavirus. J. Travel Med. *27*, taaa021.

Lu, R., Zhao, X., Li, J., Niu, P., Yang, B., Wu, H., Wang, W., Song, H., Huang, B., Zhu, N., et al. (2020). Genomic characterisation and epidemiology of 2019 novel coronavirus: implications for virus origins and receptor binding. Lancet *395*, 565–574.

Lurie, N., Saville, M., Hatchett, R., and Halton, J. (2020). Developing Covid-19 Vaccines at Pandemic Speed. N. Engl. J. Med. *382*, 1969–1973.

Mateus, J., Grifoni, A., Tarke, A., Sidney, J., Ramirez, S.I., Dan, J.M., Burger, Z.C., Rawlings, S.A., Smith, D.M., Phillips, E., et al. (2020). Selective and cross-reactive SARS-CoV-2 T cell epitopes in unexposed humans. Science *370*, 89–94.

Mercado, N.B., Zahn, R., Wegmann, F., Loos, C., Chandrashekar, A., Yu, J., Liu, J., Peter, L., McMahan, K., Tostanoski, L.H., et al. (2020). Single-shot Ad26 vaccine protects against SARS-CoV-2 in rhesus macaques. Nature *586*, 583–588.

Palm, A.E., and Henry, C. (2019). Remembrance of Things Past: Long-Term B Cell Memory After Infection and Vaccination. Front. Immunol. *10*, 1787.

Pinto, D., Park, Y.-J., Beltramello, M., Walls, A.C., Tortorici, M.A., Bianchi, S., Jaconi, S., Culap, K., Zatta, F., De Marco, A., et al. (2020). Cross-neutralization of SARS-CoV-2 by a human monoclonal SARS-CoV antibody. Nature *583*, 290–295.

Quinlan, B.D., Mou, H., Zhang, L., Guo, Y., He, W., Ojha, A., Parcells, M.S., Luo, G., Li, W., Zhong, G., et al. (2020). The SARS-CoV-2 receptor-binding domain elicits a potent neutralizing response without antibody-dependent enhancement. bioRxiv. https://doi.org/10.1101/2020.04.10.036418.

Ravichandran, S., Coyle, E.M., Klenow, L., Tang, J., Grubbs, G., Liu, S., Wang, T., Golding, H., and Khurana, S. (2020). Antibody signature induced by SARS-CoV-2 spike protein immunogens in rabbits. Sci. Transl. Med. *12*, eabc3539.

Rogers, T.F., Zhao, F., Huang, D., Beutler, N., Burns, A., He, W.-t., Limbo, O., Smith, C., Song, G., Woehl, J., et al. (2020).). Isolation of potent SARS-CoV-2 neutralizing antibodies and protection from disease in a small animal model. Science *369*, 956–963.

Sallusto, F., Lanzavecchia, A., Araki, K., and Ahmed, R. (2010). From vaccines to memory and back. Immunity *33*, 451–463.

Sanders, J.M., Monogue, M.L., Jodlowski, T.Z., and Cutrell, J.B. (2020). Pharmacologic Treatments for Coronavirus Disease 2019 (COVID-19): A Review. JAMA *323*, 1824–1836.

Shereen, M.A., Khan, S., Kazmi, A., Bashir, N., and Siddique, R. (2020). COVID-19 infection: Origin, transmission, and characteristics of human coronaviruses. J. Adv. Res. *24*, 91–98.

Shim, B.-S., Kwon, Y.-C., Ricciardi, M.J., Stone, M., Otsuka, Y., Berri, F., Kwal, J.M., Magnani, D.M., Jackson, C.B., Richard, A.S., et al. (2019). Zika Virus-Immune Plasmas from Symptomatic and Asymptomatic Individuals Enhance Zika Pathogenesis in Adult and Pregnant Mice. MBio *10*, e00758-19.

Shin, M.D., Shukla, S., Chung, Y.H., Beiss, V., Chan, S.K., Ortega-Rivera, O.A., Wirth, D.M., Chen, A., Sack, M., Pokorski, J.K., and Steinmetz, N.F. (2020). COVID-19 vaccine development and a potential nanomaterial path forward. Nat. Nanotechnol. *15*, 646–655.

Smatti, M.K., Al Thani, A.A., and Yassine, H.M. (2018). Viral-Induced Enhanced Disease Illness. Front. Microbiol. *9*, 2991.

Tian, J.-H., Patel, N., Haupt, R., Zhou, H., Weston, S., Hammond, H., Lague, J., Portnoff, A.D., Norton, J., Guebre-Xabier, M., et al. (2020). SARS-CoV-2 spike glycoprotein vaccine candidate NVX-CoV2373 elicits immunogenicity in baboons and protection in mice. bioRxiv. https://doi.org/10.1101/2020.06.29.178509.

Tokatlian, T., Read, B.J., Jones, C.A., Kulp, D.W., Menis, S., Chang, J.Y.H., Steichen, J.M., Kumari, S., Allen, J.D., Dane, E.L., et al. (2019). Innate immune recognition of glycans targets HIV nanoparticle immunogens to germinal centers. Science *363*, 649–654.

Tseng, C.T., Sbrana, E., Iwata-Yoshikawa, N., Newman, P.C., Garron, T., Atmar, R.L., Peters, C.J., and Couch, R.B. (2012). Immunization with SARS coronavirus vaccines leads to pulmonary immunopathology on challenge with the SARS virus. PLoS ONE *7*, e35421.

van Doremalen, N., Lambe, T., Spencer, A., Belij-Rammerstorfer, S., Purushotham, J.N., Port, J.R., Avanzato, V.A., Bushmaker, T., Flaxman, A., Ulaszewska, M., et al. (2020). ChAdOx1 nCoV-19 vaccine prevents SARS-CoV-2 pneumonia in rhesus macaques. Nature *586*, 578–582.

Walls, A.C., Park, Y.-J., Tortorici, M.A., Wall, A., McGuire, A.T., and Veesler, D. (2020). Structure, Function, and Antigenicity of the SARS-CoV-2 Spike Glycoprotein. Cell *181*, 281–292.e6.

Wan, Y., Shang, J., Sun, S., Tai, W., Chen, J., Geng, Q., He, L., Chen, Y., Wu, J., Shi, Z., et al. (2020). Molecular Mechanism for Antibody-Dependent Enhancement of Coronavirus Entry. J. Virol. *94*, e02015–e02019.

Wang, H., Zhang, Y., Huang, B., Deng, W., Quan, Y., Wang, W., Xu, W., Zhao, Y., Li, N., Zhang, J., et al. (2020a). Development of an Inactivated Vaccine Candidate, BBIBP-CorV, with Potent Protection against SARS-CoV-2. Cell *182*, 713–721.e9.

Wang, N., Shang, J., Jiang, S., and Du, L. (2020b). Subunit Vaccines Against Emerging Pathogenic Human Coronaviruses. Front. Microbiol. *11*, 298–298.

Wang, W., Zhou, X., Bian, Y., Wang, S., Chai, Q., Guo, Z., Wang, Z., Zhu, P., Peng, H., Yan, X., et al. (2020c). Dual-targeting nanoparticle vaccine elicits a therapeutic antibody response against chronic hepatitis B. Nat. Nanotechnol. *15*, 406–416.

Watanabe, Y., Allen, J.D., Wrapp, D., McLellan, J.S., and Crispin, M. (2020). Site-specific glycan analysis of the SARS-CoV-2 spike. Science *369*, 330–333.

Yang, J., Wang, W., Chen, Z., Lu, S., Yang, F., Bi, Z., Bao, L., Mo, F., Li, X., Huang, Y., et al. (2020). A vaccine targeting the RBD of the S protein of SARS-CoV-2 induces protective immunity. Nature *586*, 572–577.

Yu, J., Tostanoski, L.H., Peter, L., Mercado, N.B., McMahan, K., Mahrokhian, S.H., Nkolola, J.P., Liu, J., Li, Z., Chandrashekar, A., et al. (2020). DNA vaccine protection against SARS-CoV-2 in rhesus macaques. Science, eabc6284.

Zakeri, B., Fierer, J.O., Celik, E., Chittock, E.C., Schwarz-Linek, U., Moy, V.T., and Howarth, M. (2012). Peptide tag forming a rapid covalent bond to a protein, through engineering a bacterial adhesin. Proc. Natl. Acad. Sci. USA *109*, E690–E697.

Zhang, N.-N., Li, X.-F., Deng, Y.-Q., Zhao, H., Huang, Y.-J., Yang, G., Huang, W.-J., Gao, P., Zhou, C., Zhang, R.-R., et al. (2020a). A thermostable mRNA vaccine against COVID-19. Cell *182*, 1271–1283.e16.

Zhang, Y., Zhang, J., Chen, Y., Luo, B., Yuan, Y., Huang, F., Yang, T., Yu, F., Liu, J., Liu, B., et al. (2020b). The ORF8 Protein of SARS-CoV-2 Mediates Immune Evasion through Potently Downregulating MHC-I. bioRxiv, 2020.2005.2024.111823.

Zhu, F.-C., Guan, X.-H., Li, Y.-H., Huang, J.-Y., Jiang, T., Hou, L.-H., Li, J.-X., Yang, B.-F., Wang, L., Wang, W.-J., et al. (2020a). Immunogenicity and safety of a recombinant adenovirus type-5-vectored COVID-19 vaccine in healthy adults aged 18 years or older: a randomised, double-blind, placebo-controlled, phase 2 trial. Lancet *396*, 479–488.

Zhu, N., Zhang, D., Wang, W., Li, X., Yang, B., Song, J., Zhao, X., Huang, B., Shi, W., Lu, R., et al.; China Novel Coronavirus Investigating and Research Team (2020b). A Novel Coronavirus from Patients with Pneumonia in China, 2019. N. Engl. J. Med. *382*, 727–733.

STAR★METHODS

KEY RESOURCES TABLE

REAGENT or RESOURCE	SOURCE	IDENTIFIER
Antibodies		
Goat anti-Mouse IgG (H+L) Secondary Antibody, HRP	Invitrogen	Cat#31430; RRID: AB_228307
Goat anti-Monkey IgG (H+L) Secondary Antibody, HRP	Invitrogen	Cat#PA1-84631; RRID: AB_933605
Rabbit Polyclonal anti-SARS-CoV-2 Nucleoprotein (N) Antibody	Sino Biological	Cat#40143-T62
Goat Anti-Rabbit IgG Secondary Antibody (HRP)	Sino Biological	Cat#SSA004
CD3e Monoclonal Antibody (145-2C11), FITC	eBioscience	Cat#11-0031-82; RRID: AB_464882
Alexa Fluor 700 anti-mouse CD4 Antibody	Biolegend	Cat#100429; RRID: AB_493698
Brilliant Violet 510 anti-mouse CD8a Antibody	Biolegend	Cat#100752; RRID: AB_2563057
FITC anti-mouse/human CD44 Antibody	Biolegend	Cat#103006; RRID: AB_312957
PE anti-mouse CD62L Antibody	Biolegend	Cat#104407; RRID: AB_313094
PE-Cy7 Hamster Anti-mouse CD69 Antibody	BD Biosciences	Cat#552879; RRID: AB_394508
Ultra-LEAF Purified anti-mouse CD28 Antibody	Biolegend	Cat#102116; RRID: AB_11147170
APC anti-mouse IFN-γ Antibody	Biolegend	Cat#505810; RRID: AB_315404
PE anti-mouse IL-4 Antibody	Biolegend	Cat#504103; RRID: AB_315317
APC anti-mouse/human CD45R/B220 Antibody	Biolegend	Cat#103212; RRID: AB_312997
PerCP/Cyanine5.5 anti-mouse CD11c Antibody	Biolegend	Cat#117327; RRID: AB_2129642
CD209b (SIGN-R1) Monoclonal Antibody (eBio22D1 (22D1)), APC	eBioscience	Cat#17-2093-80; RRID: AB_11149350
CD11b Monoclonal Antibody (M1/70), PE-Cyanine7	eBioscience	Cat#25-0112-82; RRID: AB_469588
Brilliant Violet 421 anti-mouse CD169 (Siglec-1) Antibody	Biolegend	Cat#142421; RRID: AB_2734202
F4/80 Monoclonal Antibody (BM8), APC	Invitrogen	Cat#MF48005; RRID: AB_10375306
FITC anti-mouse IgG1 Antibody	Biolegend	Cat#406606; RRID: AB_493293
PE anti-mouse IgG2b Antibody	Biolegend	Cat#406707; RRID: AB_2563380
FITC anti-mouse CD38 Antibody	Biolegend	Cat#102705; RRID: AB_312926
Bacterial and Virus Strains		
E.coli BL21	Takara	Cat#9126
SARS-CoV-2	This paper	hCoV-19/CHN/SYSU-IHV/2020 strain; GISAID: EPI_ISL_444969
ZIKV	Dr. Bishi Fu	Strain MR766
Biological Samples		
Serum samples from BALB/c mice	This paper	N/A
Serum samples from hACE2 mice	This paper	N/A
Serum samples from rhesus macaques	This paper	N/A
Lung samples from hACE2 mice	This paper	N/A
Blood samples from healthy individuals	Guangzhou Blood Center, Guangzhou	http://www.gzbc.org/

(*Continued on next page*)

Continued

REAGENT or RESOURCE	SOURCE	IDENTIFIER
Chemicals, Peptides, and Recombinant Proteins		
4',6-Diamidino-2-Phenylindole, Dihydrochloride (DAPI)	ThermoFisher	Cat#D1306
eBioscience Fixable Viability Dye eFluor 780	Invitrogen	Cat#65-0865
Isopropyl β-D-1 thiogalactopyranoside (IPTG)	Takara	Cat#9030
Ni Sepharose excel	GE Healthcare	17-3712-01
Sigma adjuvant System (SAS)	Sigma-Aldrich	Cat#S6322
eBioscience Intracellular Fixation & Permeabilization Buffer Set	Invitrogen	Cat#88-8824
Brefeldin A	Topscience	T6062; CAS: 20350-15-6
Monensin sodium salt	Topscience	T1033; CAS: 22373-78-0
Collagenase from Clostridium histolyticum-Type IV	Sigma-Aldrich	V900893; CAS9001-12-1
ELISA Stop Solution	Solarbio	C1058
eBioscience TMB Solution	eBioscience	Cat#00-4201
Carboxymethylcellulose sodium salt (CMC)	Sigma-Aldrich	21902; CAS9004-32-4
TrueBlue HRP Substrate	KPL	50-78-02
Paraformaldehyde	Sigma-Aldrich	P6148; CAS30525-89-4
Penicillin-Streptomycin, Liquid	ThermoFisher	Cat#15140122
Fetal Bovine Serum (FBS)	ThermoFisher	Cat#10270-106
Biotin-Protein Ligase / BirA Enzyme	GeneCopoeia	BI001
Brilliant Violet 421 Streptavidin	BioLegend	Cat#405225
Recombinant SC-Ferritin protein	This paper	N/A
Recombinant ST-RBD protein	This paper	N/A
Recombinant ST-HR protein	This paper	N/A
SARS-CoV-2 Spike Glycoprotein Peptides Pool	GenScript	Cat#RP30020
HCoV-OC43 Spike glycoprotein Peptides Pool	GenScript	Cat#RP30011
HCoV-229E Spike Glycoprotein Peptides Pool	GenScript	Cat#RP30010
Recombinant Human GM-CSF	PeproTech	Cat#300-03
Recombinant Human IL-4	PeproTech	Cat#200-04
Recombinant Human TNF-α	PeproTech	Cat#300-01A
Recombinant Human IL-2	PeproTech	Cat#200-02
Recombinant Human IL-10	PeproTech	Cat#200-10
Critical Commercial Assays		
RNeasy Mini Kit	QIAGEN	Cat#74104
SARS-CoV-2 RNA detection kit (PCR-Fluorescence Probing)	Da An Gene Co.	DA0931
Monkey IFN-γ ELISPOT kit	MabTech	3421M-4AST-2
Monkey IL-4 T cell ELISPOT kit	U-Cytech	Cat#CT128-PR2
Mouse IFN-γ ELISPOT kit	Dakewe	Cat#2210005
Mouse IL-4 precoated ELISPOT kit	Dakewe	Cat#2210402
Human IFN-γ precoated ELISPOT kit	Dakewe	Cat#2110005
Pierce Rapid Gold BCA Protein Assay Kit	ThermoFisher	Cat#A53225
Luciferase Assay System	Promega	Cat#E4550

(*Continued on next page*)

Continued

REAGENT or RESOURCE	SOURCE	IDENTIFIER
Experimental Models: Cell Lines		
HEK293T	ATCC	CRL-3216; RRID: CVCL_0063
HeLa	ATCC	CCL-2; RRID: CVCL_0030
Vero E6	ATCC	CRL-1586; RRID:CVCL_0574
FreeStyle CHO-S cells	Invitrogen	Cat#R800-07
Experimental Models: Organisms/Strains		
Transgenic hACE2 mice (C57BL/6)	GemPharmatech Co, Ltd	N/A
C57BL/6 mice	Guangdong Medical Laboratory Animal Center	N/A
BALB/c mice	Guangdong Medical Laboratory Animal Center	N/A
Rhesus macaques	Guangdong Landau Biotechnology Co, Ltd	N/A
IFNαR−/− mice (C57BL/6)	Jackson Laboratory	N/A
Oligonucleotides		
SARS-CoV-2 nucleocapsid (N) qPCR Forward Primer:5′-CAGTAGGGGAACTTCTCCTGCT-3′	Da An Gene Co.	DA0931
SARS-CoV-2 nucleocapsid (N) qPCR Reverse Primer:5′-CTTTGCTGCTGCTTGACAGA-3′	Da An Gene Co.	DA0931
SARS-CoV-2 nucleocapsid (N) Probe: 5′-FAM-CTGGCAATGGCGGTGATGCTGC-BHQ1-3′	Da An Gene Co.	DA0931
Recombinant DNA		
pET28a-SC-Ferritin-6His	This paper	N/A
pcDNA3.1-SP-ST-RBD-6His	This paper	N/A
pcDNA3.1-SP-ST-HR-6His	This paper	N/A
psPAX2	Dr. Didier Trono	Addgene Plasmid #12260
pHIV-Luciferase	Dr. Bryan Welm	Addgene Plasmid #21375
SARS-CoV Spike Gene	Dr. Wenlin Huang	GenBank: AAP13567.1
MERS-CoV Spike Gene	Dr. Shibo Jiang	GenBank: AFS88936.1
HCoV-229E Spike Gene ORF cDNA clone expression plasmid	Sino Biological	Cat# VG40605-CF; GenBank: APT69883.1
HCoV-OC43 Spike Gene ORF cDNA clone expression plasmid	Sino Biological	Cat# VG40607-CF; GenBank: AVR40344.1
RATG13 Spike Gene	This paper	GenBank: QHR63300.2
Mouse CD64/FCGR1 ORF mammalian expression plasmid	Sino Biological	Cat#MG50086-ACR
Mouse CD32/Fc gamma RII/FCGR2 Gene ORF cDNA clone expression plasmid	Sino Biological	Cat#MG50030-ACG
Rhesus CD64/FCGR1 ORF mammalian expression plasmid	Sino Biological	Cat#CG90017-ACR
Cynomolgus CD32b/FCGR2B/Fc gamma RIIB Gene ORF cDNA clone expression plasmid	Sino Biological	Cat#CG90014-ACG
Software and Algorithms		
GraphPad Prism v8.0 software	GraphPad	https://www.graphpad.com/scientific-software/prism/
BD LSRFortessa cell analyzer	BD Biosciences	http://www.bdbiosciences.com/in/instruments/lsr/index.jsp
FlowJo v10	Tree Star	https://www.flowjo.com/

(*Continued on next page*)

Continued

REAGENT or RESOURCE	SOURCE	IDENTIFIER
Image Studio Lite v4.0	LI-COR Biosciences	https://www.licor.com/bio/image-studio-lite/
QuantStudio 7 Flex System	ThermoFisher	https://www.thermofisher.com/order/catalog/product/4485701#/4485701
GloMax 96 Microplate Luminometer Software v1.9.3	Promega	https://www.promega.com/resources/software-firmware/detection-instruments-software/promega-branded-instruments/glomax-96-microplate-luminometer/
SkanIt SW for Microplate Readers	ThermoFisher	https://www.thermofisher.com/order/catalog/product/5187139?SID=srch-srp-5187139
ImmunoSpot software v5.1.34	Cellular Technology Ltd	http://www.immunospot.com/ImmunoSpot-analyzers
Other		
Superose 6 Increase 10/300 GL	GE Healthcare	29091596
Amicon Ultra-15 Centrifugal Filter Unit	Millipore	UFC900396
Talos L120C microscope	ThermoFisher	https://www.thermofisher.com/cn/zh/home/electron-microscopy/products/transmission-electron-microscopes/talos-l120c-tem-ls.html
Leica RM2235	Leica	https://www.leicabiosystems.com/cn/histology-equipment/microtomes/products/leica-rm2235/
Olympus BX63	Olympus	https://www.olympus-lifescience.com.cn/zh/microscopes/upright/fluorescence/

RESOURCE AVAILABILITY

Lead Contact

Further information and requests for resources and reagents should be directed to and will be fulfilled by the Lead Contact, Dr. Hui Zhang (zhangh92@mail.sysu.edu.cn).

Materials Availability

Plasmids sequences for vaccine components will be made available upon request. Purified proteins for *in vitro* experiments can be generated upon execution of a material transfer agreement (MTA) with inquiries directed to Dr. Hui Zhang.

Data and Code Availability

The published article includes all datasets generated or analyzed during this study.

EXPERIMENTAL MODEL AND SUBJECT DETAILS

Ethics Statements

The Ethics Review Board of Sun Yat-sen University approved this study. Blood samples of healthy participants were obtained from Guangzhou Blood Center. We did not have any interaction with the healthy participants or protected information. Therefore, no informed consent was required. Animal experiments were carried out in strict compliance with the guidelines and regulations of Laboratory Monitoring Committee of Guangdong Province of China, and were approved by Ethics Committee of Zhongshan School of Medicine (ZSSOM) of Sun Yat-sen University on Laboratory Animal Care (Assurance Number: 2017-061). Authentic SARS-CoV-2 challenge studies were approved by the Ethics Committee of ZSSOM of Sun Yat-sen University on Laboratory Animal Care (Assurance Number: 2017-061) as well. Non-human primates experiments were approved by the Institutional Animal Care and Use Committee (IACUC) of Guangdong Landau Biotechnology Co,Ltd. (IACUC Approval No: LDACU 20200216-01).

Cells and Viruses

HEK293T, HeLa and Vero E6 cells were obtained from ATCC. These adherent cells were cultured in DMEM supplemented with 1% penicillin-streptomycin (ThermoFisher) and 10% FBS (ThermoFisher). Suspension FreeStyle CHO-S (Invitrogen R800-07) cells were

maintained in Freestyle CHO medium (GIBCO) supplemented with 8 mM glutamine (ThermoFisher) and 1% penicillin-streptomycin (ThermoFisher), incubated in polycarbonate vent-cap Erlenmeyer shaker ñask under 37°C, 8% CO_2 and 120 rpm speed in orbital shaker. The cell viability was maintained > 95% before transfection and the passage number were controlled to be less than 30 generations. Peripheral blood mononuclear cells (PBMCs) and primary $CD8^+$ T cells were isolated and purified from study participants and cultured in RPMI 1640 supplemented with 1% penicillin-streptomycin and 10% FBS. Primary $CD8^+$ T cells were supplied with 1/1000∼1/10000 recombinant human interleukin 2 (IL-2) (R&D) to maintain proliferation viability. Adherent cells, PBMCs and primary $CD8^+$ T cells were cultured in sterile incubator at 37°C and 5% CO_2. All cells have been tested for mycoplasma utilizing PCR assay and confirmed to be mycoplasma-free. SARS-CoV-2 (hCoV-19/CHN/SYSU-IHV/2020 strain; Accession ID on GISAID: EPI_ISL_444969) was isolated from the sputum of a female infected individual and propagated in Vero E6 cells. ZIKV strain MR766 (Rhesus/1947/Uganda) was a kindly gift from Dr. Bishi Fu. All the authentic SARS-CoV-2- and ZIKV-related experiments were conducted in a BSL-3 facility.

Animal Models

Transgenic hACE2 mice (C57BL/6) were purchased from GemPharmatech Co,Ltd. The generation procedure was described as below. hACE2 mice were generated via CRISPR/Cas9 system. First, sgRNA-targeting the mACE2 gene and donor vector with the hACE2 and mACE2 chimeric CDS was designed and constructed *in vitro*. Subsequently, Cas9, sgRNA and donor vector were co-injected into fertilized eggs of C57BL/6 mice for homologous recombination. Positive F0 mice were obtained and identified by PCR and sequencing analysis. Two primer pairs were used for genotyping: 5′-AAGTGGCTCCTCTCTTACACTCTGG-3′ and 5′-CAGCCAGGTAAATAAGGGCTCAAAG-3′ for the detection of 5¢homology recombination, and 5′-ATGAAGGCCCTCTGCACAAATGT-3′ and 5′-CCAATATCTCTGACCTTCATGGGC-3′ for the detection of 3¢homology recombination. The stable inheritable positive F1 heterozygous mice model was obtained by mating F0 mice with C57BL/6 mice. Specific-pathogen-free (SPF) 5-6-week old female BALB/c mice were purchased from Guangdong Medical Laboratory Animal Center. All mice were housed and vaccinated in SPF facilities at Laboratory Animal Center of Sun Yat-sen University. Twelve adult rhesus macaques (6 male, 6 female) between 2-4-year old were purchased from Guangdong Landau Biotechnology Co, Ltd. Monkeys experiments were conducted according to the guidelines and regulations of Laboratory Monitoring Committee of Guangdong Province of China.

METHOD DETAILS

Protein Expression and Purification

SC-Ferritin was expressed and purified from *Escherichia coli (E.coli)*. Briefly, DNA sequences of 6 × His-tagged SC-Ferritin were cloned to pET28a vector. The construct was transformed into BL21 (Takara). Single clone was amplified in LB with kanamycin at 37°C while shaking. Bacteria solution was added with isopropyl β-D-1thiogalactopyranoside (IPTG) (Takara) to induce protein expression. Another 18 h post induction, protein-expressing bacteria were harvested and lysed by sonication. The supernatants were incubated with Ni-NTA agarose (GE Healthcare) to enrich His-tagged SC-Ferritin, followed by protein elution with Imidazole-containing Tris buffer. The purified proteins were concentrated and buffer-replaced with conventional Tris buffer. The concentration of SC-Ferritin was determined by BCA assay. The bacterial endotoxins in nanoparticle were quantified by tachypleus amebocyte lysate test (less than 10 EU/dose). Coomassie blue staining, western blotting against His an Ferritin, size-exclusion chromatography (SEC), and transmission electron microscopy (TEM), were executed to confirm the purity and homogeneity.

ST-RBD and ST-HR were expressed and purified from CHO-S. Briefly, DNA sequences of 6 × His-tagged SP-ST-RBD and SP-ST-HR were cloned to pcDNA3.1vector. SP-ST-RBD- and SP-ST-HR-expressing plasmids were transfected into CHO-S cells. Seven days later, supernatants were collected and centrifuged to discard cellular debris. The cleared supernatants were passed through Ni-NTA agarose to enrich His-tagged target proteins, followed by elution with Imidazole-containing Tris buffer. The purified proteins were concentrated and buffer-replaced with conventional Tris buffer. The concentrations of ST-RBD and ST-HR were determined by BCA assay. Coomassie blue staining and western blotting against His were executed to confirm the purity.

Size-Exclusion Chromatography (SEC)

ST-RBD and ST-HR were incubated with SC-Ferritin in conventional Tris buffer, respectively. Twenty-four hours later, the ST/SC-conjugated proteins were proceeded to size-exclusion chromatography (SEC). SC-Ferritin-only formed 24-mer nanoparticles and were eluted in retention of 12 mL to 15 ml. RBD-Ferritin nanoparticles were eluted in retention of 11 mL to 14 ml. RBD and HR-chimeric nanoparticles were eluted in retention of 8 mL to 13 ml. The elution of nanoparticle was concentrated, and the concentration was measured by BCA assay. Coomassie blue staining, western blotting against His tag and Ferritin, size-exclusion chromatography (SEC), and transmission electron microscopy (TEM), were executed to confirm the purity and homogeneity.

Transmission Electron Microscopy (TEM)

Transmission electron microscopy (TEM) Grids of SC-Ferritin, RBD-Ferritin and RBD-HR-chimeric-Ferritin nanoparticles were proceeded to negative-stain electron microscopy in Shuimu BioSciences Ltd. Briefly, 5 μL of each samples (0.5 μg/ul) were applied to glow-discharged electron microscopy grids covered by a thin layer of continuous film and stained with 2% uranyl acetate, followed by imaging on Talos L120C microscope (ThermoFisher) operating at an acceleration voltage of 120kV. Images were recorded at a magnification of 73,000 × and a defocus of 1.5 μm. The particles were manually picked and two-dimensional classification was performed with EMAN2.

Animal Vaccination

For BALB/c vaccination, six BALB/c mice were subcutaneously immunized with 10 μg dose of RBD-HR nanoparticle vaccines formulated with Sigma Adjuvant System (SAS) adjuvant. Mice in the RBD nanoparticle group were immunized with equal moles of RBD-Ferritin. The moles of RBD and HR in the RBD-HR monomers group were the same as RBD-Ferritin and HR-Ferritin in the RBD-HR nanoparticle group, respectively. Mice in the RBD monomer group were immunized with equal moles of RBD as RBD-Ferritin in the RBD-HR nanoparticle group. Mice in the Ferritin group were immunized with equal moles of ferritin which were the sum of RBD-Ferritin and HR-Ferritin in the RBD-HR nanoparticle group. Equal volumes of adjuvant vaccinated mice were set as the mock group. All the mice were vaccinated with the above vaccines in a prime/boost manner which was vaccinating mice at week 0 and week 4. Serum was collected every two weeks. Mice were euthanized at week 10.

For hACE2 mice vaccination, all the mice were vaccinated as in BALB/c mice, except that there were no Ferritin-only group and RBD-only group. Mice were challenged with authentic SARS-CoV-2 two weeks post boost vaccination and euthanized one week post challenge. Serum were collected at week 0, 2, 4, 6 and 7.

For rhesus macaques vaccination, four monkeys were immunized with 50 μg of RBD-HR nanoparticle vaccine. Monkeys in the RBD nanoparticle group were immunized with equal moles of RBD-Ferritin. The moles of RBD and HR in the RBD-HR monomers group were the same as RBD-Ferritin and HR-Ferritin in the RBD-HR nanoparticle group, respectively. All monkeys were vaccinated with corresponding vaccines via intramuscular injection at week 0 and week 4. Serum were collected every two weeks. All vaccines were formulated with Sigma Adjuvant System (SAS) adjuvant.

Enzyme Linked Immunosorbent Assay (ELISA)

Recombinant ST-RBD, ST-HR and SC-Ferritin proteins were coated on high-binding 96-well plates at 2 ug/mL overnight at 4°C. After washing with PBS, plates were blocked with 5% non-fat milk/PBS for 1 h. Immunized animal serum were serially diluted and added into each well in duplicate followed by incubating at room temperature for 1 h. After washing with PBS/T (containing 1% Tween-20), the detection of antigen-specific IgG antibody in serum of BALB/c, hACE2 mice or rhesus macaques was conducted through adding HRP-conjugated goat anti-mouse or goat anti-monkey secondary antibody (Invitrogen) respectively at dilution of 1:10000 and incubating for another 1 h. After washing with PBS/T, HRP substrate TMB solution (eBioscience) was added, followed by stopping reaction with stop solution (Solarbio) after sufficient development. Absorption was measure at 450 nm. The data was analyzed using GraphPad Prism 8.0 software for non-linear regression to calculate endpoint titers.

Focus Reduction Neutralizing Test (FRNT)

Vero E6 cells were seeded in 96-well plates at a density of 2×10^4 cells per well. Cell-seeded plates were placed in cell incubator until cells reached 90% to 100% confluent. Serum of BALB/c mice, hACE2 mice and rhesus macaques in each time point was 10-fold serially diluted. Five hundred FFU of authentic SARS-CoV-2 viruses were mixed with the diluted serum in a ratio of 1:1. The serum/virus mixture was incubated at 37°C for 1 h. Cell culture medium was removed from the 96-well plate, followed by the incubating with virus/serum mixture. Plates were then incubated for 1 h at 37°C. The supernatant was removed and cells were overlaid with DMEM medium containing 1.6% CMC. The 96-well plates were placed in incubator and incubated for 24 h.

On the next day, supernatant was removed completely. Cells in each well were fixed with 200 μL of 4% paraformaldehyde for 12 h at 4°C. Fixation solution was removed, followed by washing with 200 μL PBS for 3 times. Cells were subsequently incubated with 100 μL of PBS containing 0.2% Triton X-100 and 1% BSA for 30 min. After washing with 200 μL of PBS for 3 times, cells were incubated with 50 μL of diluted primary antibody against SARS-CoV-2 nucleocapsid (N) (Sino Biological) which was 1:1000 diluted with PBS containing 1% BSA at 37°C for 1 h. After primary antibody incubation, cells within each well were washed three times with 200 μL of PBS/T (0.1% Tween-20). HRP-conjugated secondary antibody against rabbit IgG (Sino Biological) was 1:2000 diluted with PBS containing 1% BSA and incubate with cells at 37°C for 1 h. The secondary antibody was removed and washed with 200 μL PBS/T for 3 times. After washing, 50 μL of TrueBlue (KPL) was added to each well and incubated for 5 min while shaking. The supernatant was removed, followed by washing with ddH_2O twice. The residual ddH_2O was removed and imaged with ImmunoSpot microanalyzer.

The FRNT50 titer was defined as the reciprocal of serum dilution at which nAbs caused 50% inhibition of infection of cells. The inhibition was represented by the decrease of number of SARS-CoV-2-infected cells in the sample wells compared to virus control wells. Reduction rates of the serial dilution assay were analyzed by Graphpad Prism 8.0 using non-linear regression to measure the FRNT50 titer.

Surface Plasmon Resonance (SPR)

The measurements of Ferritin, RBD monomers, RBD-Ferritin nanoparticles and RBD-HR_Ferritin nanoparticles binding to hACE2 were carried out with a BIAcore T100 instrument (GE Healthcare). A BIAcore CM5 Sensor Chip and an amine coupling kit were purchased from GE Healthcare. The suitable pH value of 4.5 for hACE2 immobilization was determined. The CM5 censor chip was activated and then injected with hACE2 (2 μg/mL, in 10 mM acetate buffer, pH 4.5) for 7 min. The residual activated groups on the surfaces were blocked with an injection of ethanolamine HCl (1 M) for 7 min. Ferritin only nanoparticles, RBD only monomers, RBD-Ferritin nanoparticles and RBD-HR-Ferritin nanoparticles were diluted into different concentrations and then injected (30 μl/min). hACE2-bound protein was monitored for about 120 s for each protein. The dissociation time was 200 s with running buffer per cycle. The association rate ('on rate', Ka) and dissociation rate ('off rate', Kd) were measured, followed by the calculating of equilibrium dissociation constant ('binding constant', KD).

Inhibition of RBD Binding to hACE2

Recombinant RBD proteins were covalently conjugated with an Avi-tag signal peptide (SP) at the C terminus. Subsequently, biotin was ligated to Avi-tag with biotin-protein ligase BirA enzyme (GeneCopoeia), followed by incubating with BV421-tagged Streptavidin (Biolegend). Target cells were incubated with RBD-BV421 to track RBD-specific or RBD-binding cells. hACE2-HeLa cell line was generated through infecting HeLa cells with recombinant lentiviruses which expressing human angiotensin-converting enzyme 2 (hACE2). hACE2-positive cells were sorted by FACS. The expression of hACE2 was confirmed by western blotting. Serum of immunized BALB/c mice, which was collected at week 6, was 1:100 diluted in PBS, and incubated with RBD-BV421 probe (2 ug/mL), followed by incubating with hACE2-HeLa cells. Then cells were washed with PBS to remove unbound RBD probe. Two hours post incubating, cells were resuspended to measure fluorescence by flow cytometry (BD LSRFortessa).

Pseudotyped Virus Neutralization Assay

The neutralizing antibodies of immunized animals serum against different coronaviruses were detected through pseudotyped virus neutralization assays. Briefly, to generate lentivirus-based pseudotyped virus, HEK293T cells were co-transfected with a packaging plasmid psPAX2 (Addgene), a luciferase-expressing plasmid pHIV-Luciferase (Addgene) and a plasmid expressing spike proteins of several coronaviruses which including SARS-CoV-2 (isolate Wuhan-Hu-1, GenBank: QHD43416.1), SARS-CoV (isolate CUHK-W1, GenBank: AAP13567.1), MERS-CoV (GenBank: AFS88936.1), HCoV-229E (GenBank: APT69883.1), HCoV-OC43 (GenBank: AVR40344.1.) and RATG13 (GenBank: QHR63300.2). The expression plasmid of spike protein of SARS-CoV was a kindly gift from Dr. Wenlin Huang (Sun Yat-sen University Cancer Center). The expression plasmid of spike protein of MERS-CoV was a kindly gift from Dr. ShiBo Jiang (Fudan University). Six hours post transfection, culture medium was exchanged with fresh complete DMEM. Cell supernatant which contained pseudotyped viruses was collected 48 h post transfection and filtered through a 0.45 μm filter. The pseudotyped virus-containing supernatant was stored at −80°C and tested in titration assays to determine the dilution of pseudotyped virus in neutralization assays.

For detection of neutralizing antibody against pseudotyped SARS-CoV-2 and SARS-CoV, serially diluted serum of BALB/c mice and rhesus macaques serum were mixed with viruses and incubated at 37°C, 5% CO_2 for 1 h. The serum/virus mixtures were added into wells containing 1×10^4 hACE2-HeLa cells and went on culturing for 48 h. Cells were lysed with lysis buffer (Promega) 48 h post infection. The lysate was measured for relative luminescence units in luminometer (Promega). Serum neutralization antibody against pseudotyped MERS-CoV, HCoV-229E and RATG13 were measured as above, except that target cells were replaced with Huh7 cells. The neutralization titers of serum antibody against pseudotyped virus was analyzed using GraphPad Prism 8.0 software.

SARS-CoV-2 Infection

Specific-pathogen-free (SPF), transgenic hACE2 mice (C57BL/6), which have been prime/boost immunized with different vaccines, were challenged with authentic SARS-CoV-2 in BSL-3 facility. Littermates of the same sex were randomly assigned to un-infection or infection groups. A SARS-CoV-2 strain, named as hCoV-19/CHN/SYSU-IHV/2020 (Accession ID on GISAID: EPI_ISL_444969), was isolated from a female individual, and used to challenge mice. Mice were anaesthetized with isoflurane and inoculated intranasally with 4×10^4 FFU of SARS-CoV-2 viruses. The lungs were collected at 6 days post infection (d.p.i.). The virus stocks were obtained from the supernatant of Vero E6 after inoculation for 48 h, and the titers were determined by FRNT assay targeting nucleocapsid (N) protein. Body weight, and survival rates of each mice were measured daily.

Quantitative Reverse Transcription Polymerase Chain Reaction (qRT-PCR)

Different tissues of each mice, which included lung, myocardium, liver, spleen, kidney, cerebrum, intestine, bladder, blood, lymph node, and testis or ovary, were collected and homogenized with gentleMACS M tubes (Miltenyi Biotec, 130-093-236) in a gentleMACS dissociator (Miltenyi Biotec, 130-093-235). RNAs of homogenized tissues were extracted with RNeasy Mini Kit (QIAGEN, 74104) according to the manufacturer's instruction, followed by the qRT-PCR to determine the viral RNA copies of different tissues utilizing one-step SARS-CoV-2 RNA detection kit (PCR-Fluorescence Probing) (Da An Gene Co., DA0931). To generate a standard curve, the SARS-CoV-2 *nucleocapsid (N)* gene was cloned into a pcDNA3.1 expression plasmid and *in vitro* transcribed to obtain RNAs for standards. Indicated copies of *N* standards were 10-fold serially diluted and proceeded to qRT-PCR utilizing the same one-step SARS-CoV-2 RNA detection kit to obtain standard curves. The reactions were carried out on a QuantStudio 7 Flex System (Applied Biosystems) according to the manufacturer's instruction under the following reaction conditions: 50°C for 15 min, 95°C for 15 min, and 45 cycles of 94°C for 15 s and 55°C for 45 s. The viral RNA copies of each tissue were calculated into copies per ml and presented as log10 scale. The *N* specific primers and probes were: N-F (5′- CAGTAGGGGAACTTCTCCTGCT-3′), N-R (5′-CTTTGCTGCTGCTTGACAGA−3′) and N-P (5′-FAM-CTGGCAATGGCGGTGATGCTGC-BHQ1-3′). In each qRT-PCR experiment, both positive control and negative control of simulated RNA virus particles were included to monitor the entire experimental process and ensure the reliability of the test results.

Splenocytes Isolation and Flow Cytometry

The spleen was collected in PBS and homogenized through a 70 μm strainer, and incubated in ACK lysis buffer to remove red blood cells (RBCs), followed by passing through a 40 μm strainer to obtain single splenocytes. For the staining of T cell surface markers, cells were stained with indicated fluorochrome-conjugated monoclonal antibodies for 30 min within PBS containing 0.5% BSA on ice. LIVE/DEAD Fixable Viability Dyes (Thermo) were used to gate live cells. The following indicated antibodies were used: anti-CD3 (UCHT1), anti-CD4

(RPA-T4), anti-CD8 (OKT8), anti-CD44 (IM7), anti-CD62L (MEL-14), and anti-CD69 (H1.2F3). The gating strategies for splenocytes were described in supplemental figures.

Intracellular Cytokine Staining (ICCS)

In order to quantify the percentages of antigen-specific T cells, approximately 1 million splenocytes were seeded into each well and stimulated with SARS-CoV-2 S peptides pool, hCoV-OC43 S peptides pool and hCoV-229E S peptides pool (GenScript), respectively. Cells were co-stimulated with 2 μg/mL anti-CD28 (Biolegend) at 37°C with 5% CO_2 for 1 h. Cells were then incubated with 5 μg/mL brefeldin A (Topscience), 2 μM monensin (Topscience). DMSO was used as negative control. PMA/ionomycin was used as positive control. After a total of 6 h, the LIVE/DEAD Fixable Viability Dyes (Thermo Scientific) was used to exclude dead cells for analysis. Subsequently, cells were performed with a fixation/permeabilization kit (BD Biosciences). The following cytokine antibodies were used: anti-IFN-γ (XMG1.2), anti-TNF-α (MP6-XT22), anti-IL-2 (JES6-5H4), and anti-IL-4 (11B11). The percentages of cytokine-specific splenocytes were analyzed by flow cytometry.

DC and Macrophage Studies

C57BL/6 mice were subcutaneously injected with 2 nmol of RFP-tagged RBD and 2 nmol of RFP-tagged RBD-Ferritin, respectively. Both proteins were adjuvanted with SAS adjuvant. Four h post injection, inguinal lymph nodes of both sides were harvested and gently minced using scissors in 1% FBS in PBS buffer. Then lymph nodes were digested with 0.5 mg/mL collagenase I (Sigma) and 0.04 mg/mL DNase I (Roche) at 37°C for 1 h. Subsequently, cells were incubated in ACK lysis buffer to remove RBCs, followed by passing through a 40 μm strainer to obtain single cells. The following antibodies were used for DC and macrophage experiments: anti-B220 (RA3–6B2), anti-CD11c (N418), anti-CD11b (M1/70), anti-SIGNR1 (22D1), anti-CD169 (3D6.112), and anti-F4/80 (BM8). The percentages of RFP-positive DCs and macrophages were analyzed by flow cytometry.

For immunofluorescence assay against antigen-specific macrophages, lymph nodes were fixed with periodate–lysine–paraformaldehyde fixative buffer, followed by dehydrating in 30% sucrose twice before embedding in optimal cutting temperature compound (Sakura) and snap frozen in liquid nitrogen. Ten μm of cryosections were prepared and blocked in FACS buffer containing 1 mg/mL anti-FcγR mAb (2.4G2). Subsequently, cryosections were incubated with indicated antibodies against CD11b (M1/70). Images were captured with Olympus BX63 microscope.

Antigen-Specific MBCs Detection

Splenocytes of vaccinated BALB/c mice were harvested at six weeks post boost vaccination. Splenocytes were incubated with ACK lysis buffer to remove RBCs, followed by resuspending in cold media and immediately used for staining. Recombinant SARS-CoV-2 RBD was conjugated to BV421 as we described above. The following antibodies were used to identify antigen-specific memory B cells (MBCs): anti-B220 (RA3–6B2), anti-IgG1 (Rat IgG), anti-IgG2a/2b (RMG2b-1), anti-CD38 (90). All flow cytometry data were acquired on LSRFortessa (BD Biosciences) analyzed with FlowJo software.

In vitro Antigen Presentation

Peripheral blood mononuclear cells (PBMCs) derived from healthy donors were isolated from peripheral blood by Ficoll-Hypaque gradient separation. PBMCs were resuspended in RPMI 1640 and allowed to adhere to plates at a final concentration of 5×10^6/mL. One day later, non-adherent cells were gently removed. The left adherent cells were cultured in medium supplemented with hGM-CSF (100 ng/mL, Peprotech) and hIL-4 (100 ng/mL, Peprotech) in 5% CO2 incubator at 37°C. Every two days, one-half of the medium was replaced by fresh medium containing double concentration of hGM-CSF and hIL-4 as indicated above. Five days later, 10 ng/mL recombinant human tumor necrosis factor (hTNF-α, Peprotech) was added to the medium to induce phenotypic and functional maturation of DCs. Another two days later, DCs were pulsed with 10 μg/mL RBD or RBD-Ferritin at 37°C for 3 h before use. 2×10^6 $CD8^+$ T cells were co-cultured and stimulated with 2×10^5 autologous DCs in a 24-well plate in the presence of 10 ng/mL recombinant human interleukin-2 (hIL-2; Peprotech). The next day, recombinant human IL-10 (Peprotech) was added to the culture medium, to give a final concentration of 10 ng/mL. $CD8^+$ T cells were re-stimulated each week in the same manner. Seven days after the fourth round of re-stimulation, $CD8^+$ T cells were harvested and stimulated with SARS-CoV-2 S peptides pool (GenScript) to 'boost' the antigen-specific $CD8^+$ T cells. ELISpot assays against IFN-γ were conducted.

Enzyme-Linked Immune Absorbent Spot (ELISpot) Assay

Indicated cells were cultured with SARS-CoV-2 S peptides pool (GenScript) at a concentration of 2 μg/well for 18-24 h. Antigen specific cells of monkeys, BALB/c mice and human PBMCs were detected by Monkey IFN-γ ELISPOT kit, Monkey IL-4 ELISPOT kit, mouse IFN-γ ELISPOT kit, mouse IL-4 ELISPOT kit and Human IFN-γ ELISPOT kit (Dakewe) according to the manufacturer's protocol. Antigen-specific spots were then counted using an S6 ultra immunoscan reader (Cellular Technology Ltd.), and the number of IFN-γ- or IL-4-positive T cells was calculated by ImmunoSpot 5.1.34 software (Cellular Technology Ltd.). The number of spots was converted into the number of spots per million cells and plotted as mean ± SEM.

Histopathology and Immunohistochemistry

SARS-CoV-2-challenged hACE2 mice were euthanized in BSL-3 facility. Major tissues, which included heart, liver, spleen, lung, kidney, cerebrum, intestine, bladder, mesenteric lymph nodes and testis/ovary, were collected and fixed in 4% paraformaldehyde buffer

for 48 h, followed by embedding with paraffin. Coronal sections were performed on the cerebrum. Transverse sections were performed for the intestine and testis. Longitudinal sections were performed on all the other tissues. The sections (3-4 μm) were stained with hematoxylin and eosin (H&E). For immunohistochemistry, lung sections of each mice were deparaffinized and rehydrated with xylene and gradient alcohol. The antigen was microwave-retrieved by citric acid buffer (pH 6.0) and then quenched for endogenous peroxidases with 3% H_2O_2 for 10 min. Bovine Serum Albumin (BSA) was used to block non-specific binding sites at room temperature for 30 min. The sections were incubated with rabbit anti-SARS-CoV-2 Nucleoprotein (N) at 1:200 dilution for overnight at 4°C. Subsequently, the sections were incubated with goat anti-rabbit IgG secondary antibody (HRP) for 2 h at room temperature and stained by 3,3¢-diaminobenzidine. Finally, the sections were dyed with hematoxylin, dehydrated with gradient concentrations of ethanol, cleared with xylene and covered with neutral balsam for microscopic examination. Images were captured with Olympus BX63 microscope.

Antibody-Dependent Enhancement (ADE) Assay

To measure the antibody-dependent enhancement (ADE) of serum of different vaccine-immunized animals, HEK293T cells were transfected with FcγRI and FcγRII-expressing plasmids. Serum of adjuvant only-, BRD-HR monomer-, RBD nanoparticle- and RBD-HR nanoparticle-vaccinated hACE2 mice was collected at week 6 and 10-fold serially diluted. Diluted sera were mixed with pseudotyped SARS-CoV-2 and incubated at 37°C, 5% CO_2 for 1 h. The serum/virus mixtures were added into each wells containing 1×10^4 mFcγRI and mFcγRII-HEK293T cells and went on culturing for 48 h. Cells were lysed with lysis buffer (Promega) 48 h post infection. The lysate was measured for relative luminescence units in luminometer (Promega). Serum of vaccinated rhesus macaques was measured for ADE similarly, except that the target cells were monkey FcγRI- and monkey FcγRII-expressing HEK293T cells. To indicate the efficiency of ADE assay, we utilized serum of ZIKV-infected *Ifnar1*$^{-/-}$ mice. *Ifnar1*$^{-/-}$ mice were infected with 50 PFU of ZIKV strain MR 766. Most mice died two weeks post infection. Sera were collected from survival mice and 10-fold serially diluted. Diluted sera were mixed with pseudotyped ZIKV and incubated at 37°C, 5% CO_2 for 1 h. The serum/virus mixtures were added into each wells containing 1×10^4 mFcγRI and mFcγRII-HEK293T cells and went on culturing for 48 h. The lysate of each well was measured as above. Sera of naive mice were treat as control.

Physical Examinations and Blood Biochemical Indexes in Monkeys

Datasets of safety-related parameters were monitored before, during, and after vaccination for rhesus macaques, which included physical examinations and blood biochemical indexes. After the prime vaccination of monkey, body temperature was measured every day for a total of 40 days. Weight was measured before vaccination and every week post prime vaccination. Blood samples were collected before vaccination and at week 2, 4, 6, 8, 10, 12 post prime vaccination. Biochemical indexes were measured, which included CREA (creatinine), UA (uric acid), UREA (blood urea), TCO_2 (total CO_2), CRP (C-reactive protein), AST (aspartate aminotransferase), ALT (alanine aminotransferase), γ-GT (γ-glutamyl transpeptidase), LDH (lactate dehydrogenase), TP (total protein), ALB (albumin), GLB (globulin) and A/G (albumin/globulin ratio), for kinetics analysis.

QUANTIFICATION AND STATISTICAL ANALYSIS

All the experiments have been performed for at least three times by at least two laboratory workers. The statistical details of specific experiments, which included the statistical tests used, number of samples, mean values, standard errors of the mean (SEM) and p values derived from indicated tests, had been described in the figure legends and showed in the figures. Statistical analyses were conducted utilizing Graphpad Prism 8.0 or Microsoft Excel. Triplicate, sextuplicate and other replicate data were presented as mean ± SEM. A value of $p < 0.05$ was considered to be statistically significant and represented as asterisk (*). Value of $p < 0.01$ was considered to be more statistically significant and represented as double asterisks (**). Value of $p < 0.001$ was considered to be the most statistically significant and represented as triple asterisks (***). Value of $p < 0.0001$ was considered to be the extremely statistically significant and represented as quadruple asterisks (****). For comparison between two treatments, a Student's t test was used. For comparison between each group with the mean of every other group within a dataset containing more than two groups, one-way ANOVA with Tukey's multiple comparisons test was used. For SARS-CoV-2 ADE experiment, two-way ANOVA with Tukey's multiple comparisons test was used. For ZIKV ADE experiment, two-way ANOVA with Sidak's multiple comparisons test was used. For the comparison of highly heterogeneous data including genetic distance of RBD and HR, a Mann-Whitney *U*-test was used.

Immunity, Volume *53*

Supplemental Information

Nanoparticle Vaccines Based on the Receptor Binding Domain (RBD) and Heptad Repeat (HR) of SARS-CoV-2 Elicit Robust Protective Immune Responses

Xiancai Ma, Fan Zou, Fei Yu, Rong Li, Yaochang Yuan, Yiwen Zhang, Xiantao Zhang, Jieyi Deng, Tao Chen, Zheng Song, Yidan Qiao, Yikang Zhan, Jun Liu, Junsong Zhang, Xu Zhang, Zhilin Peng, Yuzhuang Li, Yingtong Lin, Liting Liang, Guanwen Wang, Yingshi Chen, Qier Chen, Ting Pan, Xin He, and Hui Zhang

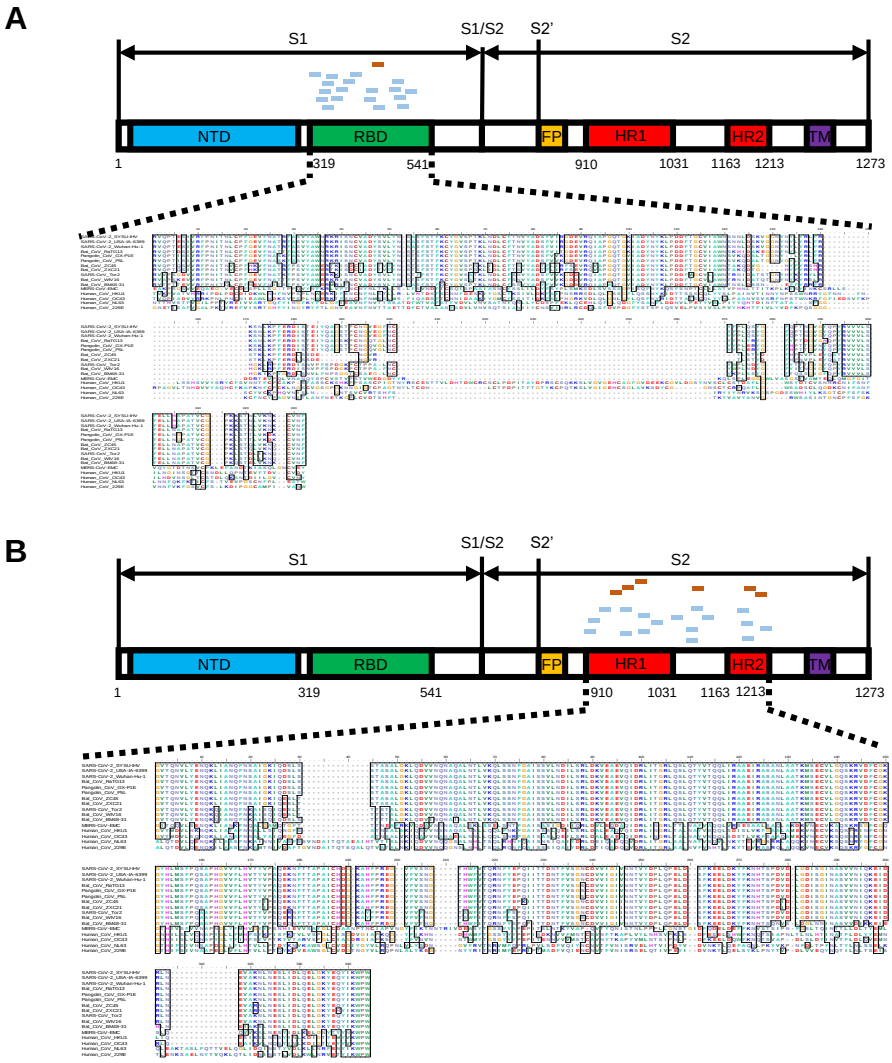
A
S1
S1/S2
S2'
S2
NTD
RBD
FP
HR1
HR2
TM
1
319
541
910
1031
1163
1213
1273
B
S1
S1/S2
S2'
S2
NTD
RBD
FP
HR1
HR2
TM
1
319
541
910
1031
1163
1213
1273

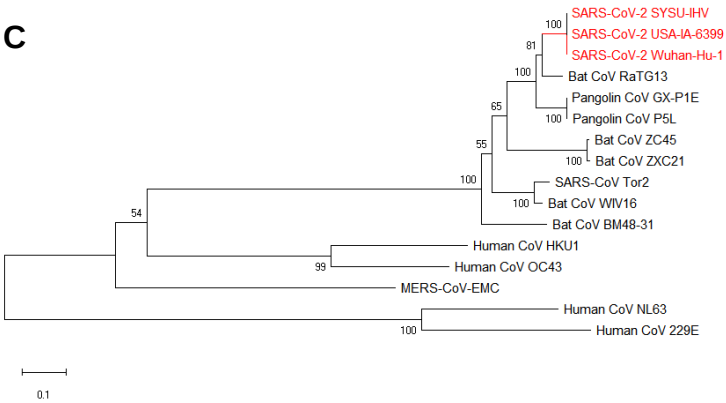
C
SARS-CoV-2 SYSU-IHV
SARS-CoV-2 USA-IA-6399
SARS-CoV-2 Wuhan-Hu-1
Bat CoV RaTG13
Pangolin CoV GX-P1E
Pangolin CoV P5L
Bat CoV ZC45
Bat CoV ZXC21
SARS-CoV Tor2
Bat CoV WIV16
Bat CoV BM48-31
Human CoV HKU1
Human CoV OC43
MERS-CoV-EMC
Human CoV NL63
Human CoV 229E
0.1

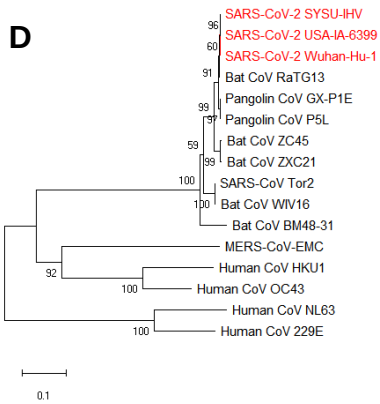
D
SARS-CoV-2 SYSU-IHV
SARS-CoV-2 USA-IA-6399
SARS-CoV-2 Wuhan-Hu-1
Bat CoV RaTG13
Pangolin CoV GX-P1E
Pangolin CoV P5L
Bat CoV ZC45
Bat CoV ZXC21
SARS-CoV Tor2
Bat CoV WIV16
Bat CoV BM48-31
MERS-CoV-EMC
Human CoV HKU1
Human CoV OC43
Human CoV NL63
Human CoV 229E
0.1

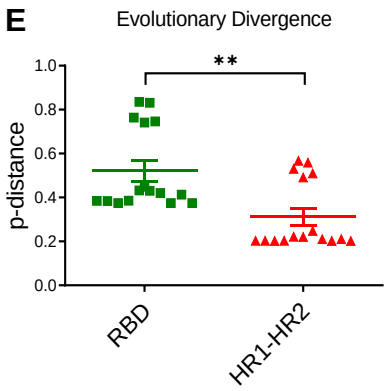
E
Evolutionary Divergence
**
p-distance
1.0
0.8
0.6
0.4
0.2
0.0
RBD
HR1-HR2

Figure S1. Related to Figure 1. Homology Analysis of RBD and HR among Coronaviruses

(A-B) Homology analysis of RBD and HR among coronaviruses which contained three SARS-CoV-2 strains (SYSU-IHV, USA-IA-6399 and Wuhan-Hu-1), six human pathogenic coronaviruses (SARS-CoV Tor2, MERS-CoV EMC, hCoV-HKU1, hCoV-OC43, hCoV-NL63 and hCoV-229E), five bat coronaviruses, and two pangolin coronaviruses. The alignments of sequences were built by using ClustalW method. All ambiguous positions were removed for each sequence pair. Orange and light blue bars within each schematic represented $CD8^+$ and $CD4^+$ T cell epitopes respectively. (C-D) The evolutionary history was inferred using the Neighbor-Joining method based on the protein sequences located in the regions of RBD:319-541(aa) (A) and HR1-HR2:910-1213(aa) (B) from the coronavirus Spike gene. The percentage of replicate trees in which the associated strains clustered together in the bootstrap test (1000 replicates) are shown next to the branches. The tree is drawn to scale, with branch lengths in the same units as those of the evolutionary distances used to infer the phylogenetic tree. (E) The average genetic distance between one given strain and the relevant entire population in the coronavirus phylogenetic tree was calculated using the p-distance method. The evolutionary analyses were performed in MEGA X software. Moreover, the two-tailed Mann-Whitney *U*-test was conducted with Prism 8.0 software for comparing the evolutionary divergence between the regions of RBD and HR1-HR2. Experiments were conducted independently in triplicates. Data represented as mean ± SEM (n=16). P-Value was calculated by two-tailed Mann-Whitney *U*-test. $^{**}p < 0.01$.

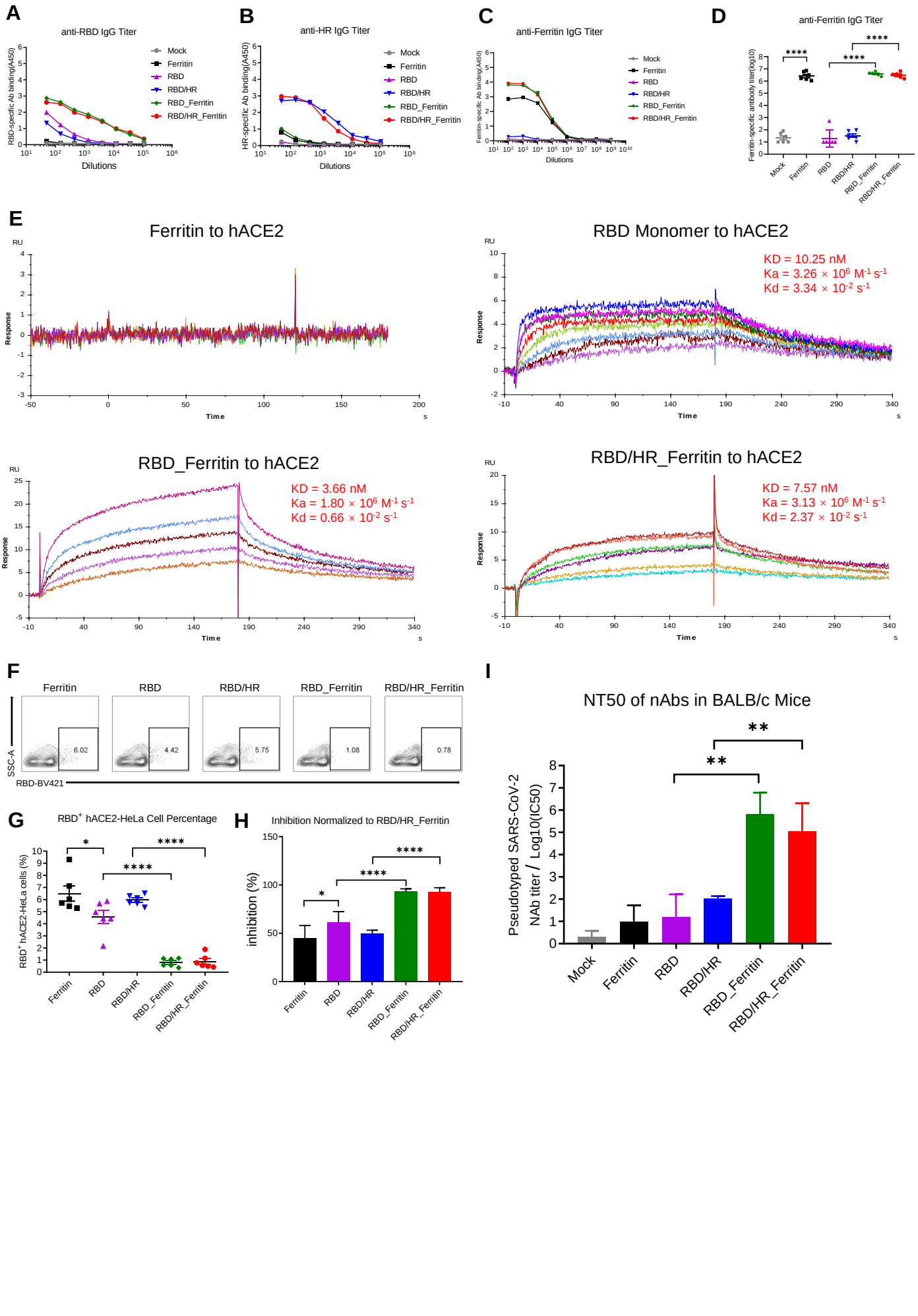
A
anti-RBD IgG Titer
RBD-specific Ab binding(A450)
Dilutions
Mock
Ferritin
RBD
RBD/HR
RBD_Ferritin
RBD/HR_Ferritin
B
anti-HR IgG Titer
HR-specific Ab binding(A450)
Dilutions
C
anti-Ferritin IgG Titer
Ferritin-specific Ab binding(A450)
Dilutions
D
anti-Ferritin IgG Titer
Ferritin-specific antibody titer(log10)
****
E
Ferritin to hACE2
RBD Monomer to hACE2
KD = 10.25 nM
Ka = 3.26 × 10^6 M^-1 s^-1
Kd = 3.34 × 10^-2 s^-1
RBD_Ferritin to hACE2
KD = 3.66 nM
Ka = 1.80 × 10^6 M^-1 s^-1
Kd = 0.66 × 10^-2 s^-1
RBD/HR_Ferritin to hACE2
KD = 7.57 nM
Ka = 3.13 × 10^6 M^-1 s^-1
Kd = 2.37 × 10^-2 s^-1
RU
Response
Time
s
F
Ferritin
RBD
RBD/HR
RBD_Ferritin
RBD/HR_Ferritin
SSC-A
RBD-BV421
6.02
4.42
5.75
1.08
0.78
G
RBD+ hACE2-HeLa Cell Percentage
RBD+ hACE2-HeLa cells (%)
H
Inhibition Normalized to RBD/HR_Ferritin
inhibition (%)
I
NT50 of nAbs in BALB/c Mice
Pseudotyped SARS-CoV-2
NAb titer / Log10(IC50)
**

Figure S2. Related to Figure 2. Humoral Immune Responses in Nanoparticles Vaccinated BALB/c Mice

(A-B) SARS-CoV-2 RBD- and HR-specific IgG titers of immunized BALB/c mice at week 6 were detected by ELISA. IgG antibody titers of serum were determined by serial dilution. (C-D) *H. pylori* ferritin-specific IgG titers of immunized BALB/c mice at week 6 were detected by ELISA and further determined by serial dilutions. The titers were represented as the reciprocal of the endpoint serum dilution (n=6). (E) Representative BIAcore plots of Ferritin, RBD monomer, RBD_Ferritin and RBD/HR_Ferritin bound to hACE2. The Ka, Kd, and KD values were calculated by the software BIAevaluation. The KD value shown was a mean of three independent experiments. (F) Serum inhibition of SARS-CoV-2 RBD binding to hACE2-HeLa cells among different groups of immunized BALB/c mice were analyzed by flow cytometry. RBD proteins were tagged by BV421. (G-H) Serum of different mice mediated RBD blocking was represented by both the percentages of RBD^+ hACE2-HeLa cells (G) and corresponding inhibition normalized to RBD/HR-Ferritin (H) (n=6). (I) Groups of serially diluted serum were detected for neutralizing antibody against pseudotyped SARS-CoV-2. Data represented NT50 of nAbs in each group. Experiments were conducted independently in triplicates. Data represented as mean ± SEM. Adjusted p-Values were calculated by one-way ANOVA with Tukey's multiple comparisons test. *$p < 0.05$, **$p < 0.01$, ***$p < 0.001$, ****$p < 0.0001$.

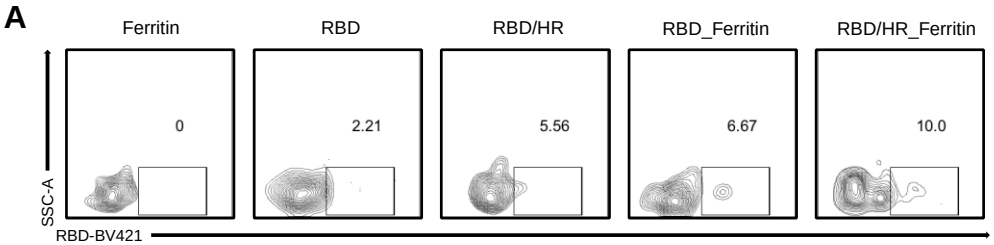
A
Ferritin
RBD
RBD/HR
RBD_Ferritin
RBD/HR_Ferritin
0
2.21
5.56
6.67
10.0
SSC-A
RBD-BV421

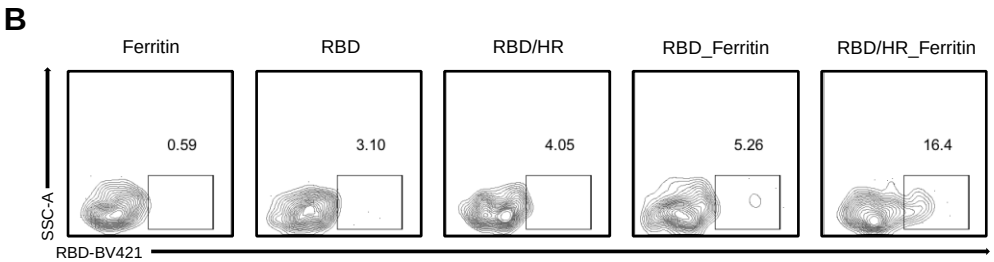
B
Ferritin
RBD
RBD/HR
RBD_Ferritin
RBD/HR_Ferritin
0.59
3.10
4.05
5.26
16.4
SSC-A
RBD-BV421

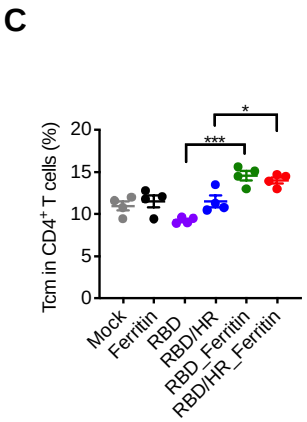
C
Tcm in CD4+ T cells (%)
Mock
Ferritin
RBD
RBD/HR
RBD_Ferritin
RBD/HR_Ferritin

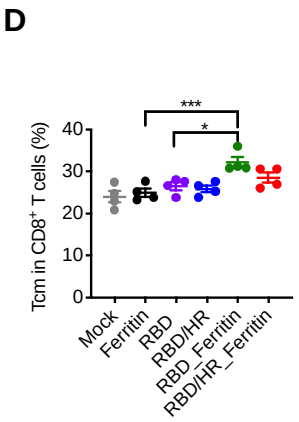
D
Tcm in CD8+ T cells (%)
Mock
Ferritin
RBD
RBD/HR
RBD_Ferritin
RBD/HR_Ferritin

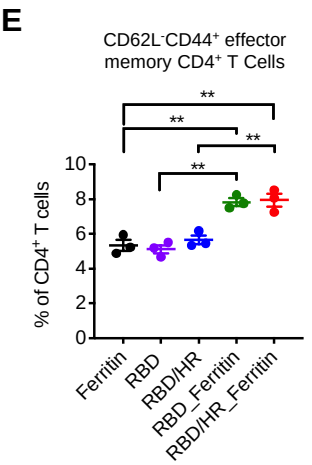
E
CD62L-CD44+ effector memory CD4+ T Cells
% of CD4+ T cells
Ferritin
RBD
RBD/HR
RBD_Ferritin
RBD/HR_Ferritin

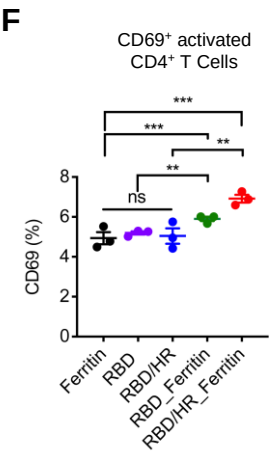
F
CD69+ activated CD4+ T Cells
CD69 (%)
ns
Ferritin
RBD
RBD/HR
RBD_Ferritin
RBD/HR_Ferritin

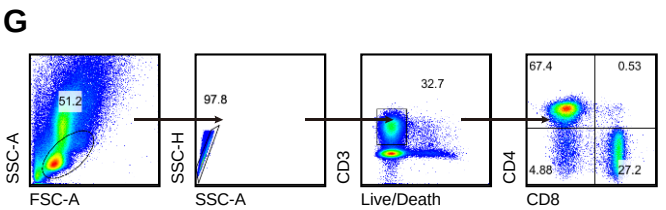
G
51.2
97.8
32.7
67.4
0.53
4.88
27.2
SSC-A
FSC-A
SSC-H
SSC-A
CD3
Live/Death
CD4
CD8

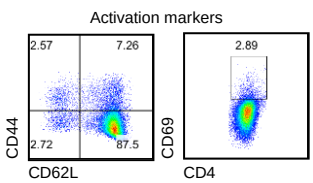
Activation markers
2.57
7.26
2.72
87.5
2.89
CD44
CD62L
CD69
CD4

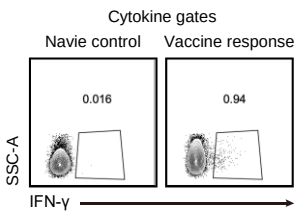
Cytokine gates
Navie control
Vaccine response
0.016
0.94
SSC-A
IFN-γ

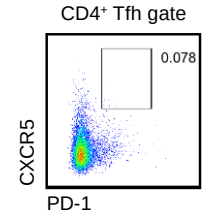
CD4+ Tfh gate
0.078
CXCR5
PD-1

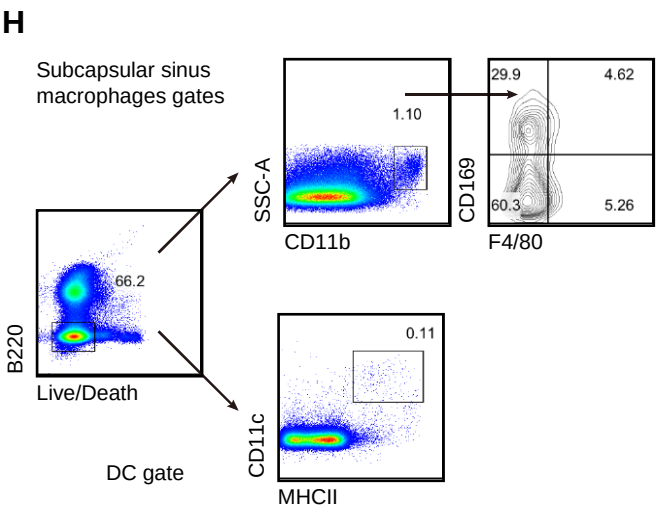
H
Subcapsular sinus macrophages gates
1.10
29.9
4.62
60.3
5.26
SSC-A
CD11b
CD169
F4/80
66.2
B220
Live/Death
DC gate
0.11
CD11c
MHCII

Figure S3. Related to Figure 2, Figure 3 and Figure 4. B and T Cell Immune Responses, Antigen Presentation and T/B Coordination

(A-B) Representative flow cytometry plots of RBD-specific IgG1 and IgG2b memory B cells. (C-D) The percentage of $CD4^+$ and $CD8^+$ central memory T cells which were isolated from spleen of 10 weeks-immunized mice were analyzed by flow cytometry (n=4). (E-F) The percentage of $CD62L^-CD44^+$ and the percentage of $CD69^+$ cells within $CD4^+$ T cells, which were isolated from spleen of 10-days immunized mice were analyzed by flow cytometry (n=3). (G) Gating strategy for activation marker staining and intracellular cytokine staining in $CD8^+$ and $CD4^+$ T cells. Activation marker were displayed. $CD8^+$ or $CD4^+$ T cells as indicated. Intracellular cytokine gating examples are spleen from a naïve mouse and a representative $CD8^+$ T cell cytokine response to antigens. (H) Gating strategy for DC and macrophage. Inguinal LNs were digested into single cells, $B220^-$ non-B cells were identified into two distinct populations: $CD11c^{hi}MHCII^+$DCs, and $CD11b^+F4/80^-CD169^+$ subscapular sinus macrophages. Experiments were conducted independently in triplicates. Data represented as mean ± SEM. Adjusted p-Values were calculated by one-way ANOVA with Tukey's multiple comparisons test. *$p < 0.05$, **$p < 0.01$, ***$p < 0.001$.

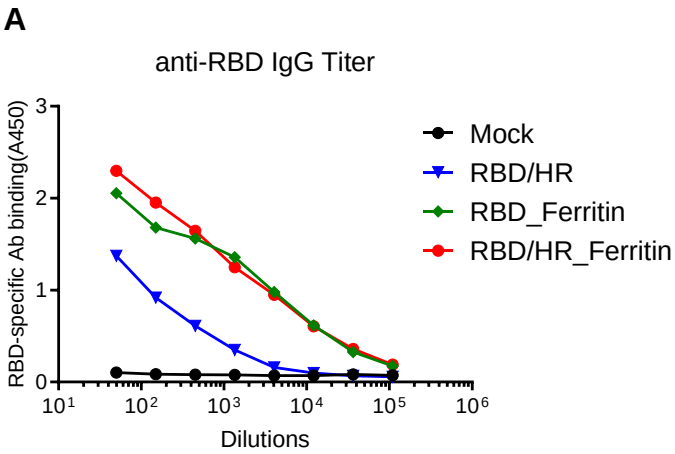
A
anti-RBD IgG Titer
RBD-specific Ab binding(A450)
Dilutions
Mock
RBD/HR
RBD_Ferritin
RBD/HR_Ferritin

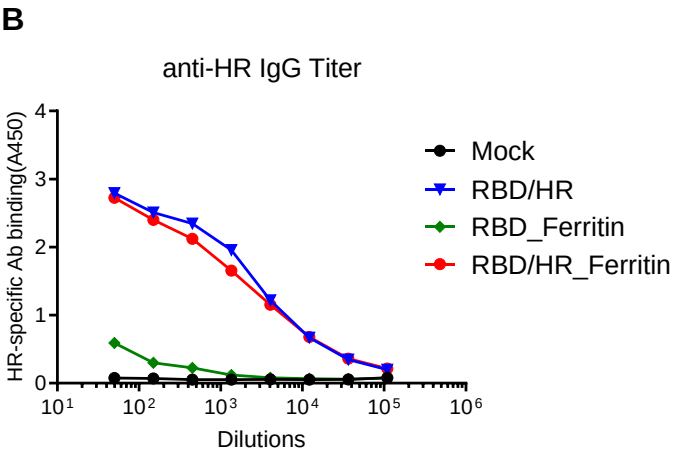
B
anti-HR IgG Titer
HR-specific Ab binding(A450)
Dilutions
Mock
RBD/HR
RBD_Ferritin
RBD/HR_Ferritin

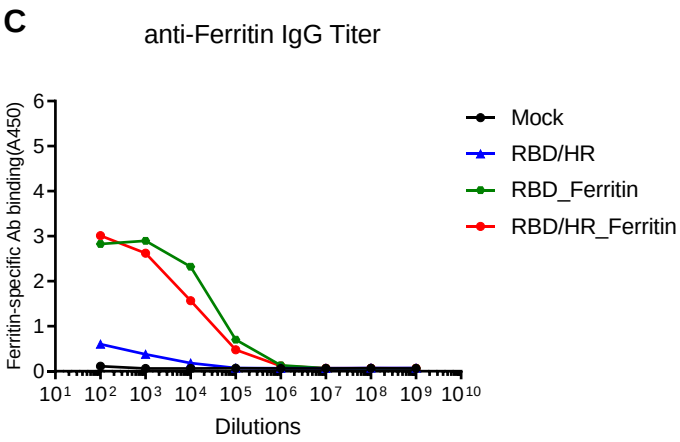
C
anti-Ferritin IgG Titer
Ferritin-specific Ab binding(A450)
Dilutions
Mock
RBD/HR
RBD_Ferritin
RBD/HR_Ferritin

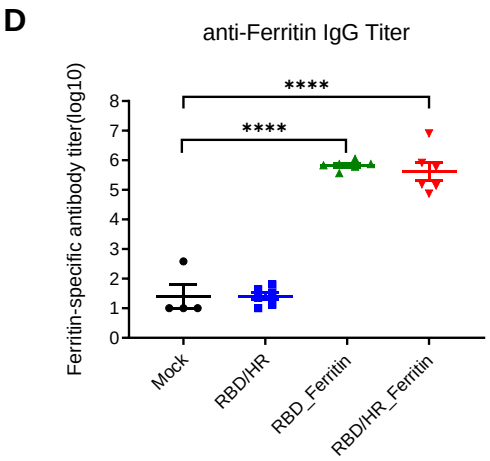
D
anti-Ferritin IgG Titer
Ferritin-specific antibody titer(log10)
****
****
Mock
RBD/HR
RBD_Ferritin
RBD/HR_Ferritin

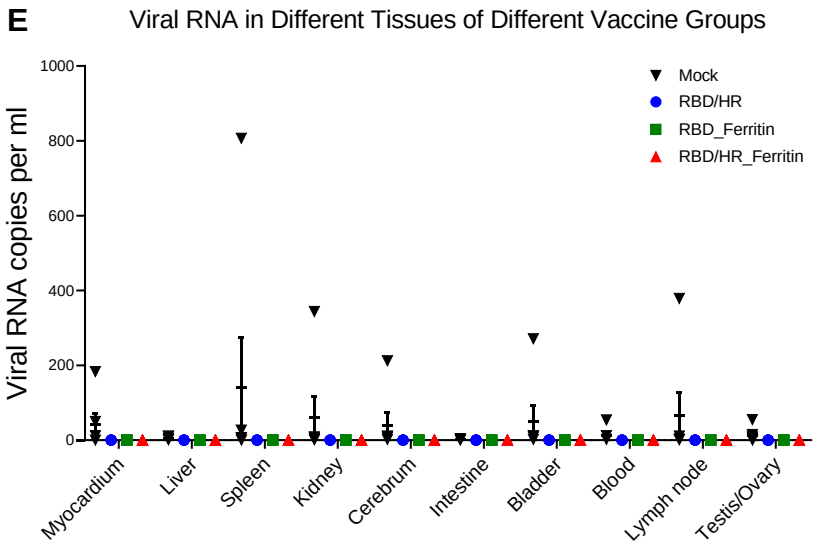
E
Viral RNA in Different Tissues of Different Vaccine Groups
Viral RNA copies per ml
Mock
RBD/HR
RBD_Ferritin
RBD/HR_Ferritin
Myocardium
Liver
Spleen
Kidney
Cerebrum
Intestine
Bladder
Blood
Lymph node
Testis/Ovary

Figure S4. Related to Figure 6. Protection of Nanoparticle Vaccines against SARS-CoV-2 in hACE2 Mice

(A-B) SARS-CoV-2 RBD- and HR-specific IgG titers of immunized hACE2 mice at week 6 were detected by ELISA. IgG antibody titers of serum were determined by serial dilution. (C-D) *H. pylori.* Ferritin-specific IgG titers of immunized hACE2 mice at week 6 were detected by ELISA and further determined by serial dilutions. The titers were represented as the reciprocal of the endpoint serum dilution. (E) Viral RNA copies in different tissues of each mice were determined by qRT-PCR and plotted as copies per ml. Experiments were conducted independently in triplicates. Data represented as mean ± SEM (n=4 for mock, n=6 for RBD/HR, RBD nanoparticle and RBD/HR nanoparticle groups). Adjusted p-Values were calculated by one-way ANOVA with Tukey's multiple comparisons test. ****$p < 0.0001$.

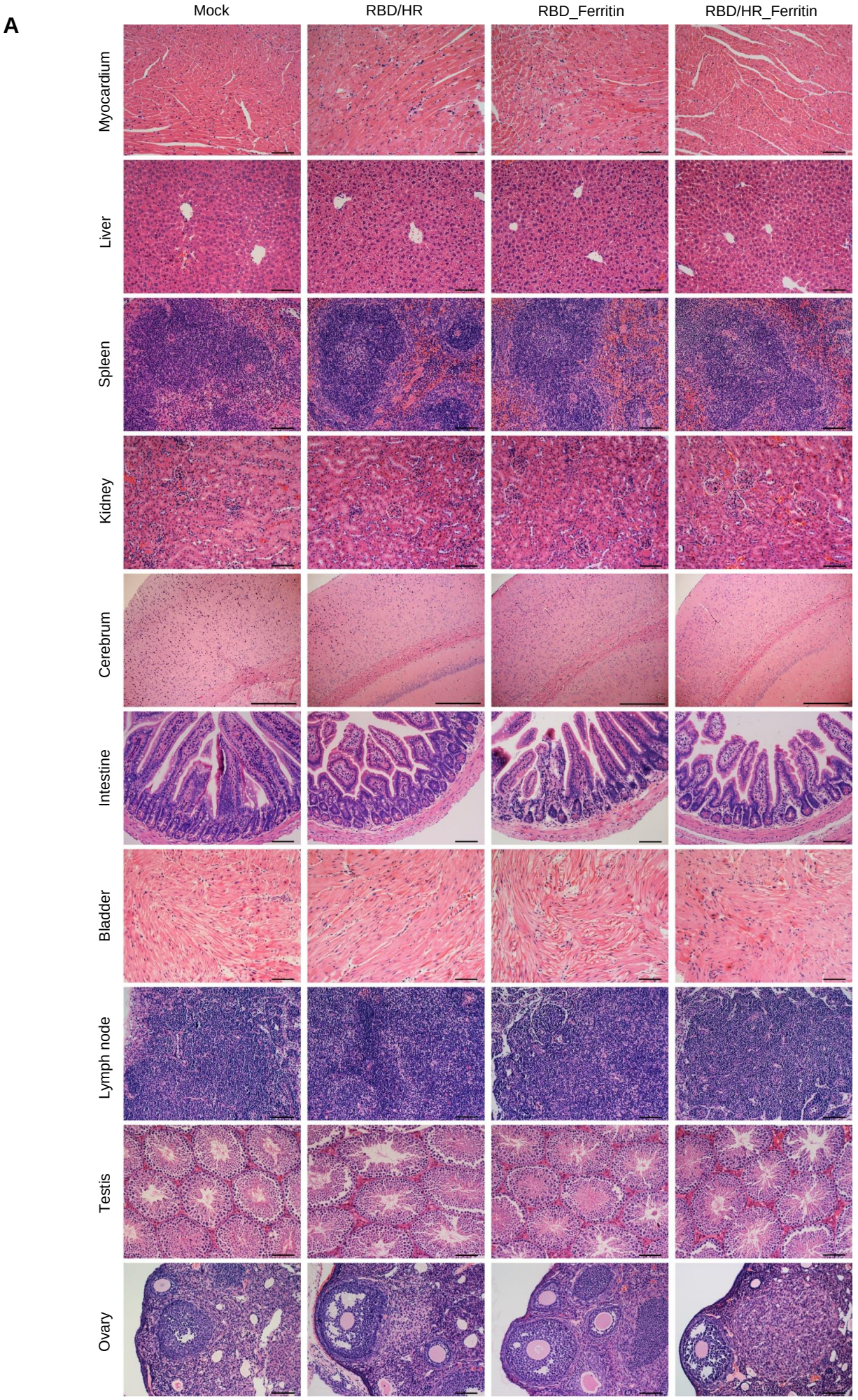
A
Mock
RBD/HR
RBD_Ferritin
RBD/HR_Ferritin
Myocardium
Liver
Spleen
Kidney
Cerebrum
Intestine
Bladder
Lymph node
Testis
Ovary

Figure S5. Related to Figure 6. Histopathological Analysis of Different Tissues of Vaccinated Mice

(A) HE staining of different tissues of vaccinated mice. Tissues contained myocardium, liver, spleen, kidney, cerebrum, intestine, bladder, lymph node, and testis or ovary. Scale bars represented 20 μm.

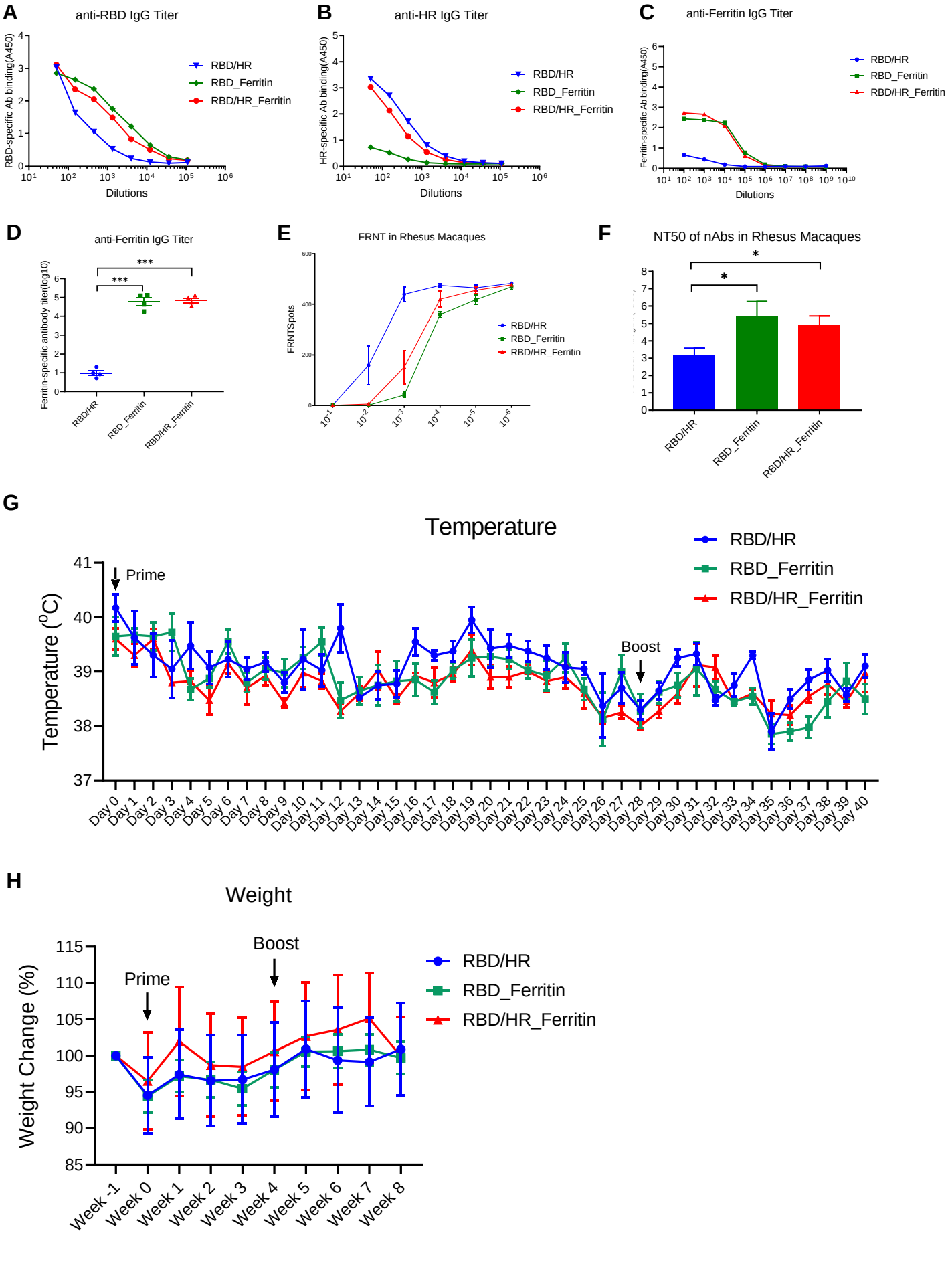
A
anti-RBD IgG Titer
RBD-specific Ab binding(A450)
Dilutions
RBD/HR
RBD_Ferritin
RBD/HR_Ferritin
B
anti-HR IgG Titer
HR-specific Ab binding(A450)
Dilutions
RBD/HR
RBD_Ferritin
RBD/HR_Ferritin
C
anti-Ferritin IgG Titer
Ferritin-specific Ab binding(A450)
Dilutions
RBD/HR
RBD_Ferritin
RBD/HR_Ferritin
D
anti-Ferritin IgG Titer
Ferritin-specific antibody titer(log10)
***
***
RBD/HR
RBD_Ferritin
RBD/HR_Ferritin
E
FRNT in Rhesus Macaques
FRNTSpots
RBD/HR
RBD_Ferritin
RBD/HR_Ferritin
F
NT50 of nAbs in Rhesus Macaques
*
*
RBD/HR
RBD_Ferritin
RBD/HR_Ferritin
G
Temperature
Temperature (°C)
Prime
Boost
RBD/HR
RBD_Ferritin
RBD/HR_Ferritin
H
Weight
Weight Change (%)
Prime
Boost
RBD/HR
RBD_Ferritin
RBD/HR_Ferritin

Figure S6. Related to Figure 7. The Immunogenicity of Nanoparticle Vaccines in Rhesus Macaques

(A-B) SARS-CoV-2 RBD- and HR-specific IgG titers of immunized rhesus macaques at week 6 were detected by ELISA. IgG antibody titers of serum were determined by serial dilution. (C-D) Ferritin-specific IgG titers of immunized monkeys at week 6 were detected by ELISA and further determined by serial dilutions. The titers were represented as the reciprocal of the endpoint serum dilution. (E) Serial dilutions of serum were analyzed by FRNT for neutralizing authentic SARS-CoV-2. (F) Groups of serially diluted serum were detected for neutralizing antibody against pseudotyped SARS-CoV-2. Data represented NT50 of nAbs in each group. (G) Body temperatures of each monkey across the whole prime/boost vaccination period. (H) Body weights of each monkey were measured every week. Experiments were conducted independently in triplicates. Data represented as mean ± SEM (n=4). Adjusted p-Values were calculated by one-way ANOVA with Tukey's multiple comparisons test. *$p < 0.05$, ***$p < 0.001$.

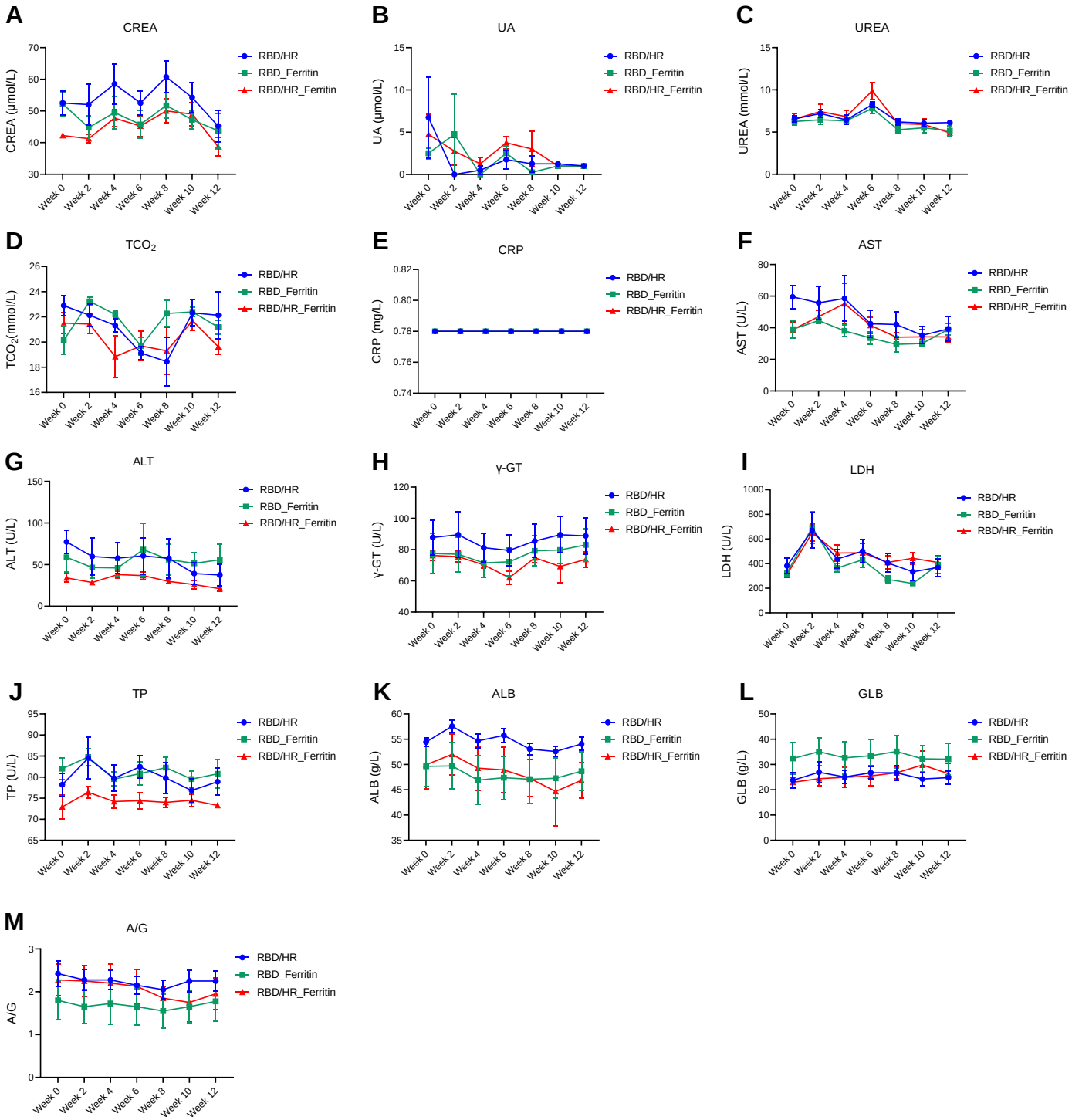
A
CREA
CREA (μmol/L)
B
UA
UA (μmol/L)
C
UREA
UREA (mmol/L)
D
TCO2
TCO2(mmol/L)
E
CRP
CRP (mg/L)
F
AST
AST (U/L)
G
ALT
ALT (U/L)
H
γ-GT
γ-GT (U/L)
I
LDH
LDH (U/L)
J
TP
TP (U/L)
K
ALB
ALB (g/L)
L
GLB
GLB (g/L)
M
A/G
A/G
RBD/HR
RBD_Ferritin
RBD/HR_Ferritin
Week 0
Week 2
Week 4
Week 6
Week 8
Week 10
Week 12

Figure S7. Related to Figure 7. Blood Biochemical Indexes of Each Vaccinated Monkey

(A-M) Blood biochemical indexes of each vaccinated monkey. The parameters contained the concentrations of creatinine (CREA), uric acid (UA), blood urea (UREA), total CO_2 (TCO_2), C-reactive protein (CRP), aspartate aminotransferase (AST), alanine aminotransferase (ALT), γ-glutamyl transpeptidase (γ-GT), lactate dehydrogenase (LDH), total protein (TP), albumin (ALB), globulin (GLB) and albumin/globulin ratio (A/G). Blood biochemical analysis was conducted every two weeks.